Title: Pattern separation of spiketrains by individual granule cells of the dentate gyrus

Authors: Antoine D. Madar*[1], Laura A. Ewell*[1,2], Mathew V. Jones[1]

[1] Department of Neuroscience, University of Wisconsin-Madison, Madison, WI 53705, USA

[2] Neurobiology Section and Center for Neural Circuits and Behavior, Division of Biological Sciences, University of California, San Diego, La Jolla, CA 92093, USA

* These authors contributed equally to the manuscript.

Corresponding authors

Mathew V. jones (mathewjones@wisc.edu)

Antoine D. Madar (madar@wisc.edu)

Abstract

Pattern separation is a process that minimizes overlap between patterns of neuronal activity representing similar experiences. Theoretical work suggests that the dentate gyrus (DG) performs this role for memory processing but a direct demonstration is lacking. One limitation is the difficulty to measure DG inputs and outputs simultaneously. To rigorously assess pattern separation by DG circuitry, we used mouse brain slices to stimulate DG afferents and simultaneously record granule cells (GCs). Output spiketrains of GCs are more dissimilar than their input spiketrains, demonstrating for the first time temporal pattern separation at the level of single neurons in DG. This phenomenon occurs from the millisecond to the second timescales through different neural codes and is not explained by simple noise. Pattern separation is cell-type specific and larger in GCs than in fast-spiking interneurons. Finally, different GCs process spiketrains differently, a mechanism that likely helps to separate patterns at the population level.

Keywords: hippocampus, similarity metrics, perforant path, time code, patch-clamp, neural noise.

Introduction

How does the brain allow us to discriminate between similar events in our past? This question is a central challenge in the neurobiology of memory and remains elusive. To prevent confusion between memories that share similar features, the brain needs to store distinct activity patterns to represent distinct memories. In the influential Hebb-Marr framework of episodic memory (McNaughton and Morris, 1987; Treves et al., 2008), representations are stored in area CA3 of hippocampus, an auto-associative network where recurrent excitatory connections facilitate recall of stored patterns in response to partial cues (McNaughton and Morris, 1987; Rolls, 2010). However, strong recurrent excitation severely limits the number of patterns that can be stored without overlap (O'Reilly and McClelland, 1994; Rolls, 2010). Such overlap would lead, when a partial cue common to several patterns is presented, to the reactivation of many patterns and thus to confusion or confabulation. To avoid these interferences, the Hebb-Marr framework proposes that redundancy between input patterns is reduced before they are stored. This process of transforming similar input patterns into less similar output patterns is termed "pattern separation" (O'Reilly and McClelland, 1994; Santoro, 2013).

Theoretical models suggest that the dentate gyrus (DG) performs pattern separation of cortical inputs before sending its differentiated outputs to CA3 (Rolls, 2010; Treves et al., 2008). Indeed, DG is ideally located to do this, receiving signals via the major projection from entorhinal cortex (EC), the perforant path (PP), and sending signals to CA3 via granule cells

(GCs) axons (Amaral et al., 2007). In addition, behavioral studies have shown that DG lesions impair mnemonic discrimination (Baker et al., 2016; Kesner et al., 2016; Kesner and Rolls, 2015; McHugh et al., 2007). However, although experimental reports have concluded that pattern separation is performed by DG (Deng et al., 2013; Leutgeb et al., 2007; Marrone et al., 2011; Neunuebel and Knierim, 2014), they only directly show that similar environments or events are represented differently in the DG. The separation could be done by upstream structures and simply be reported by DG. Hence, it is still unknown whether DG itself performs pattern separation. A rigorous demonstration would require simultaneous knowledge of the inputs arriving at DG and the processed outputs from DG to CA3 (Santoro, 2013).

Another difficulty in studying pattern separation is in defining the nature of "activity patterns". Previous studies have focused on spatial patterns of "active neurons", with little reference to the dynamics of neural activity. For example, computational models predict that DG separates overlapping populations of active EC neurons into less overlapping populations of active GCs (Myers and Scharfman, 2009; O'Reilly and McClelland, 1994; Yim et al., 2014). Immediate-early genes (IEG) expression studies have confirmed that distinct events drive plasticity in different populations of GCs (Chawla et al., 2005; Deng et al., 2013; Marrone et al., 2011) and that overlap in these representations causes mnemonic interference (Ramirez et al., 2013). In contrast, *in vivo* single-unit recordings in the DG found that similar contexts are represented by the same population of active neurons, but differences are encoded by different spatially tuned firing patterns (Leutgeb et al., 2007; Neunuebel and Knierim, 2014).

These conflicting results show that pattern separation can correspond to different computations depending on the type of patterns investigated, and that multiple forms of pattern separation could in theory be implemented by DG (Santoro, 2013). For example, because *in vivo*

recordings suggest that the same neurons are used to code different environments (Leutgeb et al., 2007; Neunuebel and Knierim, 2014), it is possible that pattern separation is performed at the level of single GCs, each disambiguating the activity patterns that it receives. Such disambiguation could be done by changing firing rates, or alternatively, by changing spike timing. Previous experimental investigations of pattern separation in DG examined population vectors of place fields averaged over minutes (Leutgeb et al., 2007; Neunuebel and Knierim, 2014), but place cells also carry information at shorter timescales (Buzsaki, 2010; Eichenbaum, 2014; Kelemen and Fenton, 2016). So far, pattern separation has not been well characterized on the scale of milliseconds, and never where patterns are explicitly afferent and efferent trains of action potentials.

Here, we test the hypothesis that DG performs pattern separation of cortical spiketrains, through single GCs, on the millisecond to second timescale. We designed a novel pattern separation assay in acute brain slices to take advantage of the experimental control afforded to slice electrophysiology. Input spiketrains of varying similarities were fed into DG via its afferents, and the output of a GC was simultaneously recorded, allowing the first direct measure of pattern separation (by comparing input similarity versus output similarity), on timescales relevant to neuronal encoding and synaptic plasticity (Buzsaki, 2010; Gutig, 2014; Rieke F., 1999; VanRullen et al., 2005).

Results

Temporal pattern separation by individual dentate granule cells

A direct test of pattern separation in single GCs requires knowledge of the similarity between input patterns arriving via the PP, and comparison with the similarity between GC output

patterns. Here, we define input and output patterns as rasters of spiketrains. Unless otherwise specified, the similarity between two spiketrains was assessed by computing their pairwise Pearson's correlation coefficient (R) using a binning window τ_w of 10 ms (see **methods**). We generated sets of input spiketrains (simulating trains of incoming cortical action potentials), with each set having an average correlation R_{input} (**methods** and **Figure 1A**). We then recorded the spiking responses of GCs to these sets of input trains delivered to PP fibers (**Figure 1B-C**) (102 recording sets from 28 GCs), allowing us to compute the average output correlation (R_{output}) (**Figure 2A-B**).

For every recording set, R_{output} was lower than the R_{input} of the associated input set, indicating a decorrelation of the output spiketrains compared to their inputs (**Figure 2C**). Because peristimulus time histograms (PSTH) are a traditional and widely used way to assess the effect of a stimulus on output spiketrains by averaging out output variability, we also computed R_{output} with PSTH instead of individual spiketrains and obtained similar results (**Figure S1**). These results are the first direct experimental evidence that single GCs, the output of DG, exhibit pattern separation. The effective decorrelation, defined as the difference between R_{input} and R_{output}, was statistically significant for every input set, but was larger when input spiketrains were highly correlated (**Figure 2D and Figure S1D**). This is consistent with the role of DG in discriminating between similar memories more than already dissimilar ones (Kesner and Rolls, 2015). Note, however, that the decorrelation normalized to R_{input} is invariant: whatever the input set, the output trains were always decorrelated to about 70% of R_{input} (**Figure 2E**). Such invariance suggests that the same decorrelating mechanism is used on all input sets.

Pearson's correlation coefficient is often used to quantify the similarity between neural activity patterns in computational models (Yim et al., 2014) and in experimental recordings

(Leutgeb et al., 2007; Neunuebel and Knierim, 2014). However, the original Hebb-Marr framework theorized pattern separation as the orthogonalization of the input patterns (Hopfield, 1982; McNaughton and Morris, 1987; Santoro, 2013). As a result, the terms "decorrelation" and "orthogonalization" are often conflated in the literature, even though they are not mathematically equivalent and have a non-linear relationship (**Figure S2D** and see **methods**). For instance, pairs of spiketrains can be uncorrelated (R = 0) without being orthogonal, or can be orthogonal without being uncorrelated (**Figure 3A-C** and **Figure S2**). To determine whether output spiketrains of GCs are truly orthogonalized, we considered spiketrains as vectors and computed the normalized dot product (NDP) between pairs of spiketrains to assess their similarity (**Figure 3A and C**). For every recording set, NDP_{output} was lower than NDP_{input}, indicating that the angle between output spiketrains was closer to a right angle (i.e., orthogonal) than their inputs (**Figure 3D-E**).

Vectors can differ by their angle, but also by their norm, which in the case of spiketrains is purely dependent on the binwise firing rates. In other words, even if neurons fire in the same time bins (relative to the start of each sweep), the number of spikes per bin can be different, as quantified by the ratio between their norms (scaling factor, SF) (**Figure 3A, 3C** and **Figure S2**). Our results show that for very similar inputs, SF_{output} is slightly lower than SF_{input} for most recording sets (**Figure 3F**). This indicates that variations in the binwise firing rate of single GCs in response to similar inputs is a potential, but weak, mechanism of pattern separation at the 10 ms timescale.

As a whole, these results are the first demonstration that input spiketrains are decorrelated in the DG at the level of single GCs, and that this form of pattern separation is mediated by high levels of orthogonalization and weak levels of scaling. As a result, even though R, NDP and SF

are not linearly related in theory, R and NDP have a near linear relationship in our dataset, as opposed to R and SF (**Figure S2E-F**).

Relevant timescales of temporal pattern separation

To measure the similarity of spiketrains we have used metrics that require binning them in time windows of a prespecified size (τ_w). Because the timescales meaningful for the brain remain uncertain, it is important to assess the separation of spiketrains for different τ_w. Our analysis shows that pattern separation, measured through R or NDP, is more pronounced at smaller timescales (e.g. 5 ms) than at larger ones (≥100 ms) (**Figure 4A-B**). However, although scaling is weak at small timescales it allows DG to perform pattern separation at larger ones (0.5-2 s) through variation of the firing rate (**Figure 4C**).

Because many previous studies suggest that spiketrains can carry information directly through the timing of individual spikes (Gutig, 2014; Rieke F., 1999; VanRullen et al., 2005), we also assessed the similarity between spiketrains using SPIKE, a binless metric purely based on spike times (Kreuz et al., 2013). Our results show that input spiketrains with very similar spike times relative to their sweep start (defined here as *synchronous* spiketrains, see **methods**), are transformed into significantly less synchronous outputs, thereby confirming that temporal pattern separation occurs through spike timing modifications in single GCs (**Figure 4D**).

Mechanism of temporal pattern separation

To determine what mechanisms might support temporal pattern separation in GCs, it is necessary to understand its dynamics first. Limiting our analysis to the first presentation of an input set revealed that outputs were already significantly decorrelated (**Figure 5A-B**). This shows that the

separation mechanism is fast, consistent with the fact that the brain generally does not have the opportunity to average repeated signals. In addition, analysis of the last presentation revealed only modestly more separation than for the first one, and only for high input correlations (**Figure 5C**), suggesting that learning to recognize the input pattern is not critical.

We also noticed that when the same input spiketrain is repeated (e.g. $R_{input} = 1$) the output spiketrains are not well correlated (as shown by the mean spiketrain reliability R_w) (**Figure 6A**), consistent with well-known neural unreliability (Dobrunz and Stevens, 1999; Mainen and Sejnowski, 1995). Thus, the simplest explanation for temporal pattern separation in single GCs is that neural communication is noisy, leading to jitter and random suppression of some spikes present in the input patterns, regardless of the identity of the input or the information it conveys (**Figure 6B**). To test this, we produced a shuffled data set and a simulated data set, both with noise statistics comparable to the original data (**Figure S3,** see **methods**). R_{output} was significantly higher in the original data (**Figure 6** and **Figure S4**), showing that purely random processes yield greater levels of pattern separation than real GCs. This is especially true for highly similar inputs, which is when pattern separation is theoretically most needed (**Figure 6E** and **Figure S4B)**. On the other hand, the spiketrain reliability R_w was significantly lower for shuffled and simulated data than in real GCs (**Figure 6D-E** and **Figure S4C**). This indicates that, in response to repetitions of the same input, GCs have less variable output patterns than if their output was entirely determined by simple random processes. It appears that there is a trade-off between achieving high levels of pattern separation and reliably transmitting information.

The conclusion that GC output is not entirely governed by simple random processes is supported by other lines of evidence. First, neural noise statistics are not good predictors of R_{output} in real GCs (**Figure S5**). Notably, consistent with the fact that SR is not well correlated

with R_{output}, the average firing rate of a GC output set is not a good predictor of the output spiketrain similarity either (**Figure S6**). Thus, even though a relationship has been established between firing rates and correlations between spiketrains (de la Rocha et al., 2007), temporal pattern separation is not achieved merely because GC output spiketrains are sparser than their inputs. Finally, when averaging out the variability between output spiketrains through the PSTH, a significant level of decorrelation is still detected (**Figure S1**).

Taken together, these results suggest that dedicated, and not simply random, mechanisms support temporal pattern separation in GCs while preserving reliable signaling about their inputs.

Fast-spiking interneurons exhibit less temporal pattern separation than GCs

Any brain system might perform either pattern separation or pattern convergence to some degree (Santoro, 2013). Thus, GCs are unlikely to be the only neurons to exhibit temporal pattern separation of spiketrains. However, we would expect pattern separation to be at its greatest in GCs, at least among DG cells, because they are the output neurons of the DG. To test this hypothesis, we performed the same pattern separation assay while recording from fast-spiking interneurons (FS) of the DG instead or in addition to a GC (20 recording sets were collected on 4 FS) (**Figure 7**). We chose FS interneurons because, like GCs, they receive strong input from the PP (Ewell and Jones, 2010). The distributions of R_{output} were significantly different between the two cell types, with the R_{output} of simultaneously recorded GCs always lower than their corresponding FS (**Figure 7D**). This indicates that FS perform lower levels of decorrelation than GCs. On the other hand, R_w is significantly higher in FS, suggesting they are more reliable than GCs, illustrating again the trade-off between reliability and separation.

FS displayed bursting (i.e. more than one output spike between two input spikes) never seen in GCs (Ewell and Jones, 2010) (**Figure 7C** and **Figure S7A, S7C**) and thus had higher firing rates than GCs (**Figure S7B, S7D**). As predicted by others (de la Rocha et al., 2007), higher firing rates in FS lead to higher correlations between their output spiketrains (**Figure S7B**). We tested whether the bursting was the reason that FS perform less pattern separation than GCs by removing all spikes in a burst except the first one from the FS data set (**Figure S7C**). The resulting dataset ("non-burst" FS: nbFS) had a much lower mean firing rate than FS (**Figure S7D**). However, the degree of correlation of output spiketrains in nbFS was still significantly higher than in GCs (**Figure S7E**). Therefore, bursting and high firing rates are not sufficient to explain the difference between FS and GCs in their ability to separate spiketrains. Interestingly, R_w was also still higher in nbFS than in GCs (**Figure S7F**), showing that the greater ability of FS to reliably transmit information is not a mere consequence of bursting or high firing rates. The high fidelity of FS in relaying input spikes (**Figure S8**) is a more likely cause of their high R_w and low level of pattern separation (**Figure S5E**).

GCs perform temporal pattern separation through distinct operations on input patterns

Pattern separation is typically considered as a population-coding process (Santoro, 2013), suggesting that different GCs should take on distinct roles in coding different patterns. To compare GCs to each other, we first assessed the correlation between spiketrains from different cells (not recorded simultaneously) in response to the same input set (**Figure 8A1**). The average correlation $R_{cell\text{-}to\text{-}cell}$ is not dependent on R_{input} and is broadly distributed but skewed towards 0 (**Figure 8A2**). This suggests that different GCs have a general tendency not to fire the same way in response to the same input spiketrain. On the contrary, FS responses are more consistent

between neurons, and FS activity is also poorly correlated with simultaneously recorded GCs (**Figure 8A3**).

Next, we analyzed whether GCs perform pattern separation to the same degree on all pairs of input spiketrains, and compared the amount of decorrelation between different GCs (**Figure 8B**). Individual GCs did not process all input spiketrains in the same way, as demonstrated by the small but significant variability in effective decorrelation for different pairs of input spiketrains (**Figure 8B2**). This variability profile was then used as a fingerprint to be compared across cells that processed the same input set. Our results suggest that different GCs, even from the same animal, can perform pattern separation of the same input spiketrains quite differently. Furthermore, the way pattern separation is performed from GC to GC is more variable and more likely to be different for highly similar input (**Figure 8B3**), which is when pattern separation is theoretically most needed.

Discussion

We report that similar input spiketrains are transformed, in GCs, into less similar output spiketrains. Our findings provide the first experimental demonstration that a form of pattern separation is performed within the DG itself and exhibited at the level of single neurons. Different cell types of the DG show different levels of pattern separation, being stronger in GCs, the output neurons of the DG to CA3, than in interneurons mediating local feedforward and feedback inhibition of GCs. Temporal pattern separation does not purely result from neural noise, but is subject to variability within and between neurons that likely supports pattern separation at the population level.

A novel way to test pattern separation

In contrast to *in vivo* experiments that have difficulty identifying recorded units with certainty (Neunuebel and Knierim, 2012) and simultaneously recording the direct inputs of these units (Deng et al., 2013; Leutgeb et al., 2007; Marrone et al., 2011; Neunuebel and Knierim, 2014), *in vitro* brain slices that preserve the lamellar connections of the hippocampus offer a more accessible platform. For example, a similar experimental setup to ours was used to show that spatially segregated inputs are represented by distinct spatiotemporal patterns in populations of DG neurons (Hyde and Strowbridge, 2012; Zylberberg et al., 2016). However, our study is the first to perform an experimental analysis of pattern separation within DG by manipulating the similarity of the inputs and comparing it to the similarity of the outputs. Such a systematic approach had so far only been done in computational studies (Aimone et al., 2009; Myers and Scharfman, 2009; Neher et al., 2015; O'Reilly and McClelland, 1994; Yim et al., 2014). Although a rigorous comparison between studies is impossible because the activity patterns they considered were defined differently, the general pattern separation behavior of those models is consistent with our results (**Figure 2C-D**). Interestingly, a detailed model of the DG incorporating some notions of single neuron dynamics and synaptic learning offers the closest match with our observations, with perfectly similar inputs not leading to perfectly similar outputs (Aimone et al., 2009).

Pattern separation through "time" codes.

Until now, most studies of pattern separation in the DG assumed that neural activity patterns were ensembles of ON/OFF neurons (Deng et al., 2013; Marrone et al., 2011; Myers and Scharfman, 2009; O'Reilly and McClelland, 1994; Rolls, 2010), sometimes considering a rate

code averaged over minutes in addition to this population code (Aimone et al., 2009; Leutgeb et al., 2007; Neher et al., 2015; Neunuebel and Knierim, 2014). Because neurons carry information at timescales shorter than minutes (Buzsaki, 2010; Eichenbaum, 2014; Kelemen and Fenton, 2016; Rieke F., 1999; VanRullen et al., 2005), and because the sparse firing of active GCs during a brief event (Diamantaki et al., 2016; Pernía-Andrade and Jonas, 2014) precludes an efficient rate code (Rieke F., 1999), we studied pattern separation at sub-second timescales.

Relevant scales are given by the time constant over which neurons can integrate synaptic inputs (Buzsaki, 2010): 10-50 ms for GCs and ~100ms for the "reader" CA3 pyramidal cells. Windows of ~10 ms and ~100 ms, corresponding to gamma and theta rhythms respectively, have been shown to organize CA neuronal assemblies (Buzsaki, 2010; Harris et al., 2003; Jezek et al., 2011; Kelemen and Fenton, 2016; Lisman and Jensen, 2013; Lisman et al., 2005). In the DG, spiketrains recorded in similar environments were less synchronous than in CA3 when considering 30-300 ms windows (Leutgeb et al., 2007). In addition, due to specific network properties allowing persistent activity, the DG might also integrate information over longer time epochs on the order of seconds (Hyde and Strowbridge, 2012; Larimer and Strowbridge, 2010; Zylberberg et al., 2016), which have been shown to be relevant in CA fields as well (Kelemen and Fenton, 2016). All this suggests that the hippocampus, and DG in particular, might convey information through multiple simultaneously relevant timescales.

Most of our results are reported at a 10 ms resolution, which corresponds approximately to the spike jitter in GCs (**Figure S3**) as well as their time constant and the gamma rhythm. This choice of temporal resolution is similar to a recent computational study of pattern separation within a DG model, which used a 20 ms resolution on short spiketrains (30 ms inputs, 200 ms outputs) (Yim et al., 2014). Furthermore, we found that GCs perform pattern separation both at

the millisecond timescale, through orthogonalization or by rearranging spike times, and at the second timescale by varying their firing rate, with a smooth transition around 100 ms (**Figure 4**). Therefore, our work demonstrates for the first time that multiple codes for pattern separation coexist within DG at simultaneously relevant timescales, consistent with a potential multiplexing of signals in the hippocampus.

Defining pattern similarity

Many methods have been designed to assess similarity between pairs of spiketrains (Cutts and Eglen, 2014; Kreuz, 2011; Lyttle and Fellous, 2011), each assuming a different definition of similarity. Because we don't know which definition is used by the brain, and given the possibility that multiple ones are relevant, it is important to maintain an agnostic approach. Our study is the first to systematically test pattern separation by considering several similarity measures that span a wide range of potential neural codes (see **methods**). The fact that conceptually different similarity measures lead to converging results bolsters our conclusion that pattern separation occurs within DG at the level of single GCs. Experiments linking mnemonic discrimination by animals with various potential forms of neural pattern separation will help pinpoint which computations are actually used in episodic memory.

Computational and physiological mechanisms of temporal pattern separation

The mechanisms supporting pattern separation within DG had so far never been experimentally investigated. The orthogonalization of sequentially presented input patterns can in theory be explained by: 1) adaptive mechanisms, involving learning and recognition of input patterns, comparison with previously stored ones and the pruning out of common features, 2) non-

adaptive (intrinsic) mechanisms, 3) or both (Friedrich and Wiechert, 2014). First, concerning adaptive mechanisms, it has been suggested that Hebbian learning could enhance population pattern separation in the DG (Fontanari et al., 1995), but computational models testing different forms of synaptic learning found that it would actually impair this type of pattern separation (Neher et al., 2015; O'Reilly and McClelland, 1994). As for temporal pattern separation, our data show that it hardly benefits from the repetition of input patterns (**Figure 5**). Second, we offer indirect evidence that non-adaptive decorrelation processes support temporal pattern separation because output patterns are always decorrelated to the same proportion (**Figure 2E**), a feat that a simple random process can achieve (**Figure S4D**), suggesting that input patterns do not need to be recognized. Third, adaptive and non-adaptive mechanisms are not mutually exclusive: previous learning over days, during the neuron maturation process, could tune single GCs only to specific input patterns, allowing rapid pattern separation (Aimone et al., 2011). Indeed, a computational study suggested that adaptive networks can mature to perform a fast, non-adaptive orthogonalization of the population activity by the decorrelation between individual information channels (Wick et al., 2010).

Adaptive or not, what is the biological source of the temporal decorrelation we observed? Synaptic and intrinsic neural noises are obvious candidates, but simple randomness was not sufficient to reproduce our results (**Figure 6 and Figure S4**). More complex and realistic noisy processes including synaptic short-term plasticity as well as inhibition might have a role. However we showed that FS, which provide both feedforward and feedback inhibition to the soma of GCs (Ewell and Jones, 2010; Hu et al., 2014), exhibit poor ability to separate spiketrains. On the other hand, their ability to relay information reliably (Hu et al., 2014) (**Figure 7** and **Figure S8**) and to precisely control spike timing in target neurons (Hu et al., 2014) might

actually provide a mechanism that counteracts noisiness in GCs, increasing the fidelity of information transmission to CA3 (while still allowing effective spiketrain separation in GCs).

The computational importance of temporal pattern separation in single cells to the population level

Although more work is needed to test whether the DG is a pattern separator at the population level, the discovery of temporal pattern separation in single GCs has strong implications for population dynamics. The fact that, in response to the same patterns, single GCs rearrange their spikes differently from sweep to sweep and from cell to cell (**Figure 8A**) may enforce very small neuronal assemblies in the DG (Buzsaki, 2010). In other words, these processes may insure that a minimal number of output neurons are active at the same time: such sparsity in active neuronal population is known, from computational studies, to be critical for efficient population pattern separation (O'Reilly and McClelland, 1994).

Materials and Methods

Animals and dissection

Horizontal slices (Bischofberger et al., 2006) of the ventral and intermediate hippocampus (400 μm) were prepared from the brains of C57BL/6 male mice 15 – 25 days old (Harlan). All procedures were approved by the University of Wisconsin Institutional Animal Care and Use Committee. Mice were anesthetized with isoflurane, decapitated, and the brain was removed quickly and placed in ice-cold cutting solution containing (in mM) 83 NaCl, 26 $NaHCO_3$, 2.5 KCl, 1 $NaH2PO_4$, 0.5 $CaCl_2$, 3.3 MgCl2, 22 D-Glucose and 72 Sucrose, bubbled with 95% O_2 and 5% CO_2. Horizontal slices were cut using a vibratome (Leica VT1000S) and placed in an

incubation chamber in standard artificial cerebrospinal fluid (aCSF) containing (in mM) 125 NaCl, 25 NaHCO3, 2.5 KCl, 1.25 NaH2PO4, 2 CaCl2, 1 MgCl2, and 25 D-Glucose (or in a 50/50 mix of cutting solution and standard aCSF) at 35° C, for 15-30 minutes after dissection. Slices were stored in the incubation chamber at room temperature for at least 30 minutes before being used for recordings.

Electrophysiology

All recordings were done in aCSF. Whole cell patch-clamp recordings were made using an upright microscope (Axioskop FS2, Zeiss, Oberkochen, Germany) with infra-red differential interference contrast optics. Patch pipettes pulled from thin-walled borosilicate glass (World Precision Instruments, Sarasota, FL) had a resistance of 3-5 MΩ when filled with intracellular solution containing (in mM) 140 K-gluconate, 10 EGTA, 10 HEPES, 20 phosphocreatine, 2 Mg_2ATP, 0.3 NaGTP (pH 7.3, 310 mOsm). Recordings were done at physiological temperature (33-35 °C) using one or two Axopatch 200B amplifiers (Axon Instruments, Foster City, CA), filtered at 5 kHz using a 4-pole Bessel filter and digitized at 10 kHz using a Digidata 1320A analog-digital interface (Axon Instruments). Data were acquired to a Macintosh G4 (Apple Computer, Cupertino, CA) using Axograph X v1.0.7 (AxographX.com). Stimulation pipettes were pulled from double barrel borosillicate theta-glass (~10 µm tip diameter, Harvard Apparatus, Edenbridge, U.K.) and filled with ACSF or a 1M NaCl solution and connected to a constant current stimulus isolator used to generate 0.1-10 mA pulses, 100 microseconds in duration. GCs used for analysis (n = 28) were stable across a whole recording session as judged by monitoring of series resistance and resting potential, with the following characteristics: series resistance (R_s): 6.65 ± 0.68 MΩ; resting potential (V_{rest}): -69.3 ± 1.3 mV (min = -80 mV, max = -

51 mV); input resistance (R_i): 171 ± 16MΩ (min = 81 MΩ, max = 325 MΩ) and capacitance (C_m): 23 ± 2 pF (min = 12 pF, max = 65 pF). FS interneurons (n = 4) were identified as neurons with large somata at the hilus-granule cell layer border and a high firing rate response during large depolarizing current steps (Ewell and Jones, 2010; Harney and Jones, 2002) (Fig. 7). They had the following characteristics: R_s: 7.2 ± 1.2 MΩ; V_{rest}: -66.7 ± 3.5 mV (min = -72 mV, max = -55 mV); R_i: 59 ± 10 MΩ (min = 41 MΩ, max = 92 MΩ) and C_m: 19 ± 3 pF (min = 13 pF, max = 30 pF).

Pattern separation experiments

Input patterns were 2 second long traces of impulses simulating cortical spiketrains, with interspike intervals following a Poisson distribution of mean frequency ~10 Hz (11.9 ± 0.7 Hz, min = 9.6 Hz, max = 14.5 Hz). Firing rates were chosen to be consistent with the frequency of EPSCs recorded in GCs of behaving mice (Pernía-Andrade and Jonas, 2014), and are known to promote a high probability of spiking in GCs in slices (Andersen et al., 1966; Ewell and Jones, 2010). Eleven sets of five input trains were designed so that the 5 trains of each set would have a prespecified average correlation coefficient R_{input} when using a binning window τ_w of 10 ms. The relative standard error of the input set similarity was on average 4% of the mean for R_{input} at τ_w = 10 ms, and it was similarly constrained for other time resolutions and similarity metrics. Five sets were designed with an algorithm developed in-house (at τ_w = 10ms, R_{input} = 0.88, 0.84, 0.73, 0.65, 0.56) and six other sets were designed using the algorithm of Macke and colleagues (Macke et al., 2009) (at τ_w = 10ms, R_{input} = 1.00, 0.95, 0.76, 0.48, 0.25, 0.11). Because results did not qualitatively differ when considering data obtained from the two groups of input sets, we pooled them together for our analysis.

The spiking response of a DG neuron was recorded in whole-cell mode while stimuli were delivered to the outer molecular layer (OML). Stimulus current intensity and location were set so that the recorded neuron spiked occasionally in response to electrical impulses and the stimulation electrode was at least 100 µm away from the expected location of the dendrites of the recorded neuron. Once stimulation parameters were set, a pattern separation protocol was run. It consisted of a sequence of the five different input spiketrains, delivered one after the other separated by 4 s of relaxation, repeated ten times. The ten repetitions of the sequence of five patterns were implemented to take into account any potential variability in the output, and the non-random sequential scheme was used to avoid repeating the same input spiketrain close in time. Each protocol yielded a recording set consisting of fifty output spiketrains, each associated with one of the five different input spiketrains (**Figure 1C**). V_{rest} was maintained around -70mV during recordings, consistent with the V_{rest} of mature GCs recorded in behaving mice (Pernía-Andrade and Jonas, 2014). The output spiking frequency was variable (6.3 ± 0.3Hz, see **Figure S6**) but consistent with sparse activity generally observed in GCs *in vivo* (Danielson et al., 2016; Diamantaki et al., 2016; Leutgeb et al., 2007; Neunuebel and Knierim, 2014; Pernía-Andrade and Jonas, 2014) and in slices under conditions of drive comparable to what was used here (Dieni et al., 2016; Marin-Burgin et al., 2012).

Similarity metrics

Similarity between spiketrains was assessed in four ways: 1) with the Pearson's correlation coefficient (R), 2) with the normalized dot product (NDP), 3) with the scaling factor (SF) and 4) with a distance metric called SPIKE specifically designed to assess the dissimilarity between two spiketrains (Kreuz et al., 2013). The SPIKE-metric is a binless metric based on spike times,

whereas R, NDP and SF are based on the number of spikes occurring in time bins of prespecified durations (e.g. $\tau_w = 10$ ms).

For R, two spiketrains X and Y of the same duration, divided into N time bins of size τ_w are seen as variables, with X_i and Y_i the observations, i.e. the respective numbers of spikes in bin i for each spiketrain. R assesses the similarity between X and Y by measuring the goodness of fit of a linear regression to the distribution of points (X_i, Y_i): when R is close to 1 spiketrains are similar, close to 0 they are dissimilar and close to -1 they are anticorrelated (**Figure 3A-B)**. R was computed with the following equation, where *cov* is the covariance, σ is the standard deviation and $\bar{X}$ and $\bar{Y}$ are the means of X and Y):

$$R = \frac{cov(X,Y)}{\sigma_X . \sigma_Y} = \frac{\sum_{i=1}^{N}(X_i - \bar{X}).(Y_i - \bar{Y})}{\sqrt{\sum_{i=1}^{N}(X_i - \bar{X})^2} . \sqrt{\sum_{i=1}^{N}(Y_i - \bar{Y})^2}}$$

NDP and SF are similarity metrics explicitly considering spiketrains as vectors. They, like R, require arbitrarily dividing spiketrains into time bins, which are considered dimensions of an N-dimensional space where N is the number of bins. For two binned spiketrains X and Y, NDP is the cosine of the angle θ between the two vectors: 0 when they are perfectly orthogonal, 1 when they are collinear (**Figure 3A, 3C**). The NDP is defined as the scalar product of X and Y divided by their norms, and was computed with the following equation (where X_i and Y_i are the coordinates of X and Y, measuring the number of spikes in bin *i*):

$$\text{NDP} = \cos(\theta) = \frac{\sum_{i=1}^{N} X_i . Y_i}{\sqrt{\sum_{i=1}^{N} X_i^2} . \sqrt{\sum_{i=1}^{N} Y_i^2}}$$

SF, on the other hand, quantifies the difference of length between the two vectors X and Y, or, in other words, the variation in the binwise firing rate between two spiketrains. We have defined it as the ratio between the norms of each vector, the smaller norm always divided by the bigger one to have SF values ranging from 0 to 1. When norms ||X||, ||Y|| or both were 0 (i.e. spiketrains without spikes), SF was excluded from further analysis. SF = 1 means X and Y are identical in terms of binwise spike number. The closer to 0 SF is, the more dissimilar are the binwise firing rates (**Figure 3A, 3C**). SF was computed with the following equation (where 0 < ||X|| < ||Y||):

$$SF = \frac{\sqrt{\sum_{i=1}^{N} X_i^2}}{\sqrt{\sum_{i=1}^{N} Y_i^2}}$$

Comparing the three equations above, the relationships between R, NDP and SF are not trivial and not linear. Note that R is actually an NDP, but of vectors centered to their respective mean, which doesn't conserve the angular relationship between X and Y. To further evaluate the relationship between R, NDP and SF, we generated a set of 1012 spike rasters (1000 were random, 12 were specific cases) between which we computed the similarity with the three metrics above. Each raster was made of six bins, each bin containing 0, 1 or 2 spikes (drawn from a uniform distribution for the randomly generated group). This analysis confirmed that the three metrics are not equivalent and provides an intuition on what each metric represents (**Figure S2D**).

As explained above, R, NDP and SF are binned measures of specified size τ_w. In other words, in all the equations above, Xi and Yi are functions of τ_w and the values of the respective similarity metrics are dependent on τ_w as well. In **Figure 4**, we evaluated the influence of τ_w on the results by varying it between 5 ms and 2000 ms. Note that because our spiketrains are 2 seconds long, using τ_w = 2000 ms means the spiketrains can be seen as variables with only one observation, or as unidimensional vectors that can only vary by their norm. Thus, R is meaningless, NDP is necessarily 1, which indicates collinearity, and SF correctly assesses the variation in the overall firing rate between the two spiketrains. This analysis therefore explores a wide range of coding strategies between a temporal code with 5 ms resolution and a pure rate code.

Being binned metrics, R, NDP and SF also have the drawback of considering all X_i (i.e. bins) as independent observations, which may not be a realistic assumption. The binless SPIKE similarity metric avoids this limitation. SPIKE also differs from the other measures by not assuming that spiketrains are related linearly, or that they belong to a Euclidean space (Aronov and Victor, 2004). To compute SPIKE, we used the Matlab toolbox provided at **www.fi.isc.cnr.it/users/thomas.kreuz/sourcecode.html** which computes the SPIKE-distance (called D(t) in our study and S(t) in the original paper: see equation 19) (Kreuz et al., 2013). The SPIKE similarity was computed as: SPIKE = $1 - \frac{1}{T}\int_0^T D(t)dt$, where T is the duration of the spiketrain. Because D(t) ranges from 0 to 1, SPIKE is thus also between 0 and 1, like NDP and SF. When SPIKE is equal to 1, spiketrains have exactly the same spike times, i.e. they are synchronous (n.b. in our experiments, spiketrains were not simultaneously recorded, but we use "synchronous" in the sense of spiketrains aligned to the start of each 2 s sweep). Note that SPIKE has a large dynamic range (i.e. sensitivity over large difference of spiketimes), and, as a result,

realistic spiketrains like in our input sets rarely have a SPIKE similarity lower than 0.5 (Kreuz et al., 2013) (**Figure 4C**).

$-1 \leq R \leq 1$
$0 \leq NDP \leq 1$
$0 < SF \leq 1$
$0 \leq$ SPIKE-similarity ≤ 1; but ≥ 0.5 in most cases

Noise parameters

We define the spike-wise neural noise as the delay of an output spike after an input spike, its average jitter and its spiking reliability (SR, below) which is linked to the rate of failure to spike after an input spike. To assess these parameters, we computed the cross-occurrence between input spikes and output spikes in a [-15 ms, 50ms] interval with 1 ms bins, for each recording set. The resulting histogram of counts of output spikes occurring in the vicinity of an input spike was fitted with a Gaussian distribution $N(\mu,\sigma$, baseline), where μ is the mean delay of an output spike and σ is the jitter of this delay. The baseline corresponds to the background firing, occurring by chance or caused by neighboring inputs. After subtracting the baseline and extracting the probability of spiking by dividing the counts of output spikes by the total number of input spikes, we defined the *spiking reliability* (SR) as the sum of probabilities of an output spike in the predefined time interval around an input spike (**Figure 6B** and **Figure S3A**).

Simulated and shuffled data

To assess the role of spike-wise neural noise in pattern separation, we generated two data sets. First, we simulated output spiketrains in response to our 11 input sets (10 simulated output sets of 50 synthetic spiketrains per input set). This simulation was entirely based on the average spike-wise noise parameters computed from the real GC recordings (see above): the matrix of input spike times was replicated ten times, and for each of the 50 resulting sweeps, spikes were deleted randomly following a binomial distribution B(Number of spikes, 1-mean SR = 1-0.42). A random delay, sampled from a Gaussian distribution $N(\mu,\sigma)$, was added to each resulting spike times, with μ and σ being respectively the mean delay and mean jitter in the original recordings. The noise statistics of the resulting simulated data set is shown in **Figure S3C.**

Second, we created a surrogate data set by randomly shuffling the output spikes of the original GC recordings: the delay of each spike was conserved but it was relocated to follow a randomly selected input spike in the same input train (from a uniform distribution). This strategy yielded a data set with noise statistics closer to the original data (**Figure S3D)**.

Software and Statistics

Data analysis was performed using custom-written routines in Matlab (Mathworks, Natick, MA, USA), including functions from toolboxes cited above. Sample sizes were chosen based on the literature and estimations of the variance and effect size from preliminary data. All values are reported as mean ± S.E.M. unless otherwise noted. The one-sample Kolmogorov-Smirnov test was used to verify the normality of data distributions. Parametric or non-parametric statistical tests (see figure legends and statistic table below) were appropriately used to assess significance (p-value < 0.05). Assumptions on equal variances between groups were avoided when necessary. All T and U tests were two-tailed. To determine whether two distributions of data points are

significantly different (e.g. R_{output} as a function of R_{input}, for GC compared to FS, see **Fig. 5, 6, S4, 7, S7**), we performed a regression (linear or parabolic) on the two data sets as well as on the combined data sets, and assessed significance via an F-test comparing the goodness of fits (Motulsky and Ransnas, 1987). Because R_{input} can also be considered as a categorical variable, we performed two-way ANOVA before using post-hoc tests correcting for multiple comparisons in order to determine at which R_{input} groups two conditions were significantly different. All statistical details can be found in the statistics table at the end.

Author contributions

M.V.J conceptualized this work. L.A.E. and M.V.J. designed the experiments. L.A.E. and A.D.M. collected the data. A.D.M. performed the analysis with M.V.J. oversight. A.D.M. wrote the manuscript and all authors discussed the results, edited the manuscript and approved the final version.

Competing Interests

The authors declare no competing interests.

References

Aimone, J. B., Deng, W., & Gage, F. H. (2011). Resolving new memories: a critical look at the dentate gyrus, adult neurogenesis, and pattern separation. *Neuron, 70*(4), 589-596. doi: 10.1016/j.neuron.2011.05.010

Aimone, J. B., Wiles, J., & Gage, F. H. (2009). Computational influence of adult neurogenesis on memory encoding. *Neuron, 61*(2), 187-202. doi: 10.1016/j.neuron.2008.11.026

Amaral, D. G., Scharfman, H. E., & Lavenex, P. (2007). The dentate gyrus: fundamental neuroanatomical organization (dentate gyrus for dummies). *163*, 3-22 788-790. doi: 10.1016/s0079-6123(07)63001-5

Andersen, P., Holmqvist, B., & Voorhoeve, P. E. (1966). Excitatory synapses on hippocampal apical dendrites activated by entorhinal stimulation. *Acta Physiol Scand, 66*(4), 461-472. doi: 10.1111/j.1748-1716.1966.tb03224.x

Aronov, D., & Victor, J. D. (2004). Non-Euclidean properties of spike train metric spaces. *Physical Review E, 69*(6), 061905.

Baker, S., Vieweg, P., Gao, F., Gilboa, A., Wolbers, T., Black, S. E., & Rosenbaum, R. S. (2016). The Human Dentate Gyrus Plays a Necessary Role in Discriminating New Memories. *Curr Biol*. doi: 10.1016/j.cub.2016.07.081

Bischofberger, J., Engel, D., Li, L., Geiger, J. R., & Jonas, P. (2006). Patch-clamp recording from mossy fiber terminals in hippocampal slices. *Nat Protoc, 1*(4), 2075-2081. doi: 10.1038/nprot.2006.312

Buzsaki, G. (2010). Neural syntax: cell assemblies, synapsembles, and readers. *Neuron, 68*(3), 362-385. doi: 10.1016/j.neuron.2010.09.023

Chawla, M. K., Guzowski, J. F., Ramirez-Amaya, V., Lipa, P., Hoffman, K. L., Marriott, L. K., . . . Barnes, C. A. (2005). Sparse, environmentally selective expression of Arc RNA in the upper blade of the rodent fascia dentata by brief spatial experience. *Hippocampus, 15*(5), 579-586. doi: 10.1002/hipo.20091

Cutts, C. S., & Eglen, S. J. (2014). Detecting pairwise correlations in spike trains: an objective comparison of methods and application to the study of retinal waves. *J Neurosci, 34*(43), 14288-14303. doi: 10.1523/jneurosci.2767-14.2014

Danielson, N. B., Kaifosh, P., Zaremba, J. D., Lovett-Barron, M., Tsai, J., Denny, C. A., . . . Hen, R. (2016). Distinct contribution of adult-born hippocampal granule cells to context encoding. *Neuron, 90*(1), 101-112.

de la Rocha, J., Doiron, B., Shea-Brown, E., Josic, K., & Reyes, A. (2007). Correlation between neural spike trains increases with firing rate. *Nature, 448*(7155), 802-806. doi: 10.1038/nature06028

Deng, W., Mayford, M., & Gage, F. H. (2013). Selection of distinct populations of dentate granule cells in response to inputs as a mechanism for pattern separation in mice. *Elife, 2*, e00312. doi: 10.7554/eLife.00312

Diamantaki, M., Frey, M., Berens, P., Preston-Ferrer, P., & Burgalossi, A. (2016). Sparse activity of identified dentate granule cells during spatial exploration. *Elife, 5*. doi: 10.7554/eLife.20252

Dieni, C. V., Panichi, R., Aimone, J. B., Kuo, C. T., Wadiche, J. I., & Overstreet-Wadiche, L. (2016). Low excitatory innervation balances high intrinsic excitability of immature dentate neurons. *Nat Commun, 7*, 11313. doi: 10.1038/ncomms11313

Dobrunz, L. E., & Stevens, C. F. (1999). Response of hippocampal synapses to natural stimulation patterns. *Neuron, 22*(1), 157-166.

Eichenbaum, H. (2014). Time cells in the hippocampus: a new dimension for mapping memories. *Nat Rev Neurosci, 15*(11), 732-744. doi: 10.1038/nrn3827

Ewell, L. A., & Jones, M. V. (2010). Frequency-tuned distribution of inhibition in the dentate gyrus. *J Neurosci, 30*(38), 12597-12607. doi: 10.1523/jneurosci.1854-10.2010

Fontanari, J., Rolls, E., & Costa, D. F. (1995). A model of the operation of the hippocampus and entorhinal cortex in memory. *International Journal of Neural Systems, 6*(1), 51-70.

Friedrich, R. W., & Wiechert, M. T. (2014). Neuronal circuits and computations: pattern decorrelation in the olfactory bulb. *FEBS Lett, 588*(15), 2504-2513. doi: 10.1016/j.febslet.2014.05.055

Gutig, R. (2014). To spike, or when to spike? *Curr Opin Neurobiol, 25*, 134-139. doi: 10.1016/j.conb.2014.01.004

Harney, S. C., & Jones, M. V. (2002). Pre- and postsynaptic properties of somatic and dendritic inhibition in dentate gyrus. *Neuropharmacology, 43*(4), 584-594.

Harris, K. D., Csicsvari, J., Hirase, H., Dragoi, G., & Buzsaki, G. (2003). Organization of cell assemblies in the hippocampus. *Nature, 424*(6948), 552-556. doi: 10.1038/nature01834

Hopfield, J. J. (1982). Neural networks and physical systems with emergent collective computational abilities. *Proc Natl Acad Sci U S A, 79*(8), 2554-2558.

Hu, H., Gan, J., & Jonas, P. (2014). Interneurons. Fast-spiking, parvalbumin(+) GABAergic interneurons: from cellular design to microcircuit function. *Science, 345*(6196), 1255263. doi: 10.1126/science.1255263

Hyde, R. A., & Strowbridge, B. W. (2012). Mnemonic representations of transient stimuli and temporal sequences in the rodent hippocampus in vitro. *Nat Neurosci, 15*(10), 1430-1438. doi: 10.1038/nn.3208

Jezek, K., Henriksen, E. J., Treves, A., Moser, E. I., & Moser, M. B. (2011). Theta-paced flickering between place-cell maps in the hippocampus. *Nature, 478*(7368), 246-249. doi: 10.1038/nature10439

Kelemen, E., & Fenton, A. A. (2016). Coordinating different representations in the hippocampus. *Neurobiol Learn Mem, 129*, 50-59. doi: 10.1016/j.nlm.2015.12.011

Kesner, R. P., Kirk, R. A., Yu, Z., Polansky, C., & Musso, N. D. (2016). Dentate gyrus supports slope recognition memory, shades of grey-context pattern separation and recognition memory, and CA3 supports pattern completion for object memory. *Neurobiol Learn Mem, 129*, 29-37. doi: 10.1016/j.nlm.2015.08.010

Kesner, R. P., & Rolls, E. T. (2015). A computational theory of hippocampal function, and tests of the theory: new developments. *Neurosci Biobehav Rev, 48*, 92-147. doi: 10.1016/j.neubiorev.2014.11.009

Kreuz, T. (2011). Measures of spike train synchrony. *Scholarpedia, 6*(10). http://www.scholarpedia.org/article/Measures_of_spike_train_synchrony doi:10.4249

Kreuz, T., Chicharro, D., Houghton, C., Andrzejak, R. G., & Mormann, F. (2013). Monitoring spike train synchrony. *J Neurophysiol, 109*(5), 1457-1472. doi: 10.1152/jn.00873.2012

Larimer, P., & Strowbridge, B. W. (2010). Representing information in cell assemblies: persistent activity mediated by semilunar granule cells. *Nat Neurosci, 13*(2), 213-222. doi: 10.1038/nn.2458

Leutgeb, J. K., Leutgeb, S., Moser, M. B., & Moser, E. I. (2007). Pattern separation in the dentate gyrus and CA3 of the hippocampus. *Science, 315*(5814), 961-966. doi: 10.1126/science.1135801

Lisman, J. E., & Jensen, O. (2013). The theta-gamma neural code. *Neuron, 77*(6), 1002-1016. doi: 10.1016/j.neuron.2013.03.007

Lisman, J. E., Talamini, L. M., & Raffone, A. (2005). Recall of memory sequences by interaction of the dentate and CA3: a revised model of the phase precession. *Neural Netw, 18*(9), 1191-1201. doi: 10.1016/j.neunet.2005.08.008

Lyttle, D., & Fellous, J. M. (2011). A new similarity measure for spike trains: sensitivity to bursts and periods of inhibition. *J Neurosci Methods, 199*(2), 296-309. doi: 10.1016/j.jneumeth.2011.05.005

Macke, J. H., Berens, P., Ecker, A. S., Tolias, A. S., & Bethge, M. (2009). Generating spike trains with specified correlation coefficients. *Neural Comput, 21*(2), 397-423. doi: 10.1162/neco.2008.02-08-713

Mainen, Z. F., & Sejnowski, T. J. (1995). Reliability of spike timing in neocortical neurons. *Science, 268*(5216), 1503-1506.

Marin-Burgin, A., Mongiat, L. A., Pardi, M. B., & Schinder, A. F. (2012). Unique processing during a period of high excitation/inhibition balance in adult-born neurons. *Science, 335*(6073), 1238-1242. doi: 10.1126/science.1214956

Marrone, D. F., Adams, A. A., & Satvat, E. (2011). Increased pattern separation in the aged fascia dentata. *Neurobiol Aging, 32*(12), 2317 e2323-2332. doi: 10.1016/j.neurobiolaging.2010.03.021

McHugh, T. J., Jones, M. W., Quinn, J. J., Balthasar, N., Coppari, R., Elmquist, J. K., . . . Tonegawa, S. (2007). Dentate gyrus NMDA receptors mediate rapid pattern separation in the hippocampal network. *Science, 317*(5834), 94-99. doi: 10.1126/science.1140263

McNaughton, B. L., & Morris, R. G. M. (1987). Hippocampal synaptic enhancement and information storage within a distributed memory system. *Trends in Neuroscience, 10*(10), 408-415.

Motulsky, H. J., & Ransnas, L. A. (1987). Fitting curves to data using nonlinear regression: a practical and nonmathematical review. *FASEB J, 1*(5), 365-374.

Myers, C. E., & Scharfman, H. E. (2009). A role for hilar cells in pattern separation in the dentate gyrus: a computational approach. *Hippocampus, 19*(4), 321-337. doi: 10.1002/hipo.20516

Neher, T., Cheng, S., & Wiskott, L. (2015). Memory storage fidelity in the hippocampal circuit: the role of subregions and input statistics. *PLoS Comput Biol, 11*(5), e1004250. doi: 10.1371/journal.pcbi.1004250

Neunuebel, J. P., & Knierim, J. J. (2012). Spatial firing correlates of physiologically distinct cell types of the rat dentate gyrus. *J Neurosci, 32*(11), 3848-3858. doi: 10.1523/JNEUROSCI.6038-11.2012

Neunuebel, J. P., & Knierim, J. J. (2014). CA3 retrieves coherent representations from degraded input: direct evidence for CA3 pattern completion and dentate gyrus pattern separation. *Neuron, 81*(2), 416-427. doi: 10.1016/j.neuron.2013.11.017

O'Reilly, R. C., & McClelland, J. L. (1994). Hippocampal conjunctive encoding, storage, and recall: avoiding a trade-off. *Hippocampus, 4*(6), 661-682. doi: 10.1002/hipo.450040605

Pernía-Andrade, Alejandro J., & Jonas, P. (2014). Theta-Gamma-Modulated Synaptic Currents in Hippocampal Granule Cells In Vivo Define a Mechanism for Network Oscillations. *Neuron, 81*(1), 140-152. doi: 10.1016/j.neuron.2013.09.046

Ramirez, S., Liu, X., Lin, P. A., Suh, J., Pignatelli, M., Redondo, R. L., . . . Tonegawa, S. (2013). Creating a false memory in the hippocampus. *Science, 341*(6144), 387-391. doi: 10.1126/science.1239073

Rieke F., W. W., de Ruyter van Steveninck R., Bialek W. (1999). *Spikes: Exploring the Neural Code* (A Bradford Book).

Rolls, E. T. (2010). A computational theory of episodic memory formation in the hippocampus. *Behav Brain Res, 215*(2), 180-196. doi: 10.1016/j.bbr.2010.03.027

Santoro, A. (2013). Reassessing pattern separation in the dentate gyrus. *Front Behav Neurosci, 7*, 96. doi: 10.3389/fnbeh.2013.00096

Treves, A., Tashiro, A., Witter, M. P., & Moser, E. I. (2008). What is the mammalian dentate gyrus good for? *Neuroscience, 154*(4), 1155-1172. doi: 10.1016/j.neuroscience.2008.04.073

VanRullen, R., Guyonneau, R., & Thorpe, S. J. (2005). Spike times make sense. *Trends Neurosci, 28*(1), 1-4. doi: 10.1016/j.tins.2004.10.010

Wick, S. D., Wiechert, M. T., Friedrich, R. W., & Riecke, H. (2010). Pattern orthogonalization via channel decorrelation by adaptive networks. *J Comput Neurosci, 28*(1), 29-45. doi: 10.1007/s10827-009-0183-1

Yim, M. Y., Hanuschkin, A., & Wolfart, J. (2014). Intrinsic rescaling of granule cells restores pattern separation ability of a dentate gyrus network model during epileptic hyperexcitability. *Hippocampus*. doi: 10.1002/hipo.22373

Zylberberg, J., Hyde, R. A., & Strowbridge, B. W. (2016). Dynamics of robust pattern separability in the hippocampal dentate gyrus. *Hippocampus, 26*(5), 623-632. doi: 10.1002/hipo.22546

Figures and Legends

8 main figures, each one followed by its legend
8 satellite figures related to one or more main figures, each followed by its legend.

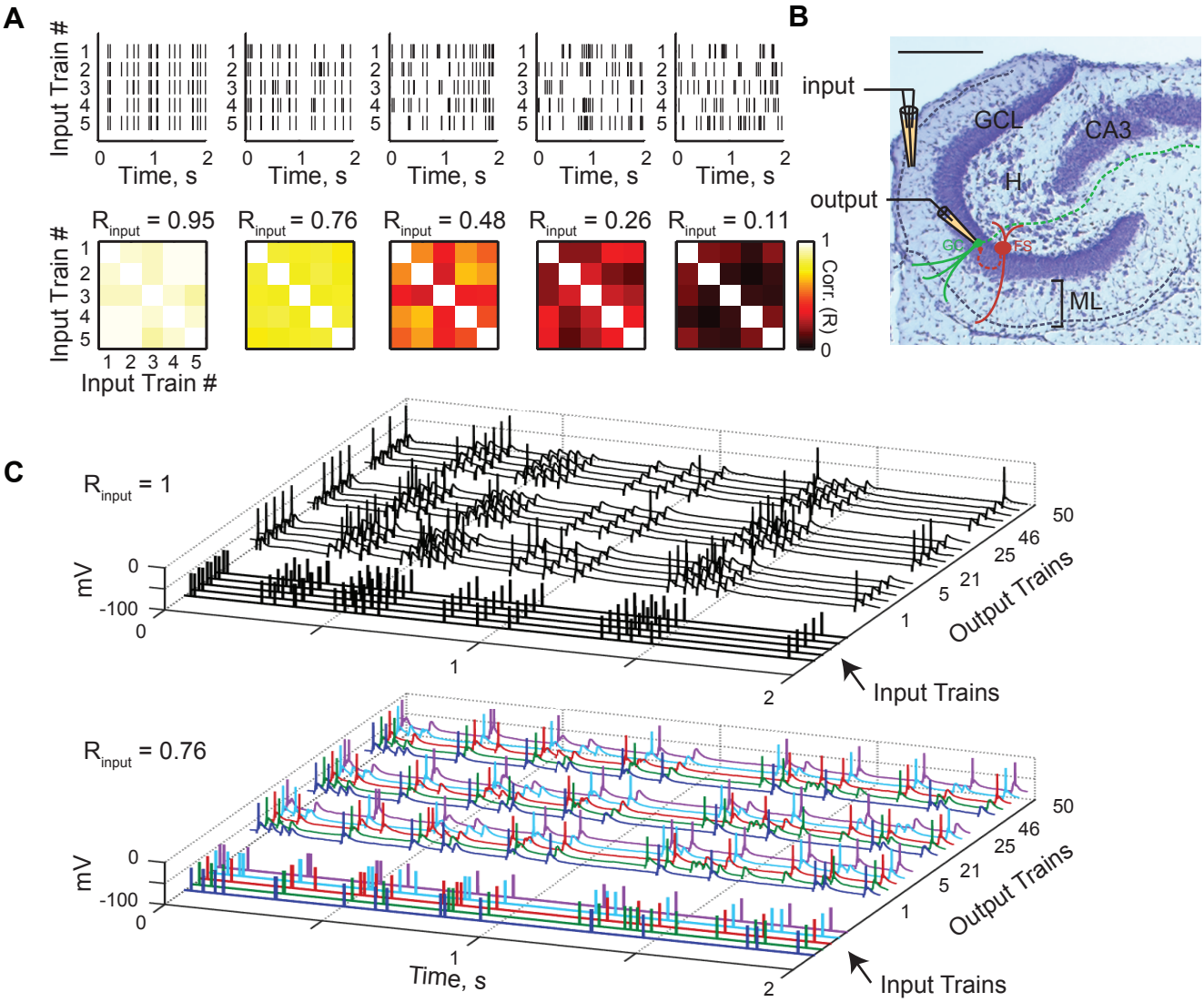
A
Input Train #
Time, s
R_{input} = 0.95
R_{input} = 0.76
R_{input} = 0.48
R_{input} = 0.26
R_{input} = 0.11
Corr. (R)
B
input
output
GCL
CA3
H
GC
FS
ML
C
R_{input} = 1
mV
Output Trains
Input Trains
R_{input} = 0.76
Time, s

Figure 1

Figure 1. Pattern separation assay in acute brain slices at the single cell level.

(A) Five input sets out of eleven used. *Top*: rasters of the five spiketrains of each set. *Bottom*: correlation coefficient matrix for each input set, each square representing the correlation coefficient between two input spiketrains measured with a binning window of 10 ms (color scale at left). Traces are ordered by decreasing similarity (i.e. coefficient average, diagonal excluded) from R_{input} = 0.95 (far left) to R_{input}=0.11 (far right).

(B) Histology of the DG in a horizontal slice (Cresyl violet/Nissl staining; scale bar: 250µm), overlaid with a schematic of the experimental setup: a theta pipette in the ML (input) is used to focally stimulate the PP while a responding GC (output) is recorded via whole-cell patch-clamp. (GCL: granule cell layer, H: hilus, ML: molecular layer, FS: fast-spiking interneuron. Solid lines represent dendrites and dashed lines axons)

(C) Current-clamp recordings of the membrane potential of two different GCs in response to different input sets (*Top*: R_{input} = 1; *Bottom*: R_{input} = 0.76). Each set of five input traces is repeated ten times (only 3 sweeps are shown, with amplitudes truncated at 0 mV). In the bottom graph, input trains and their respective children output spiketrains have matching colors.

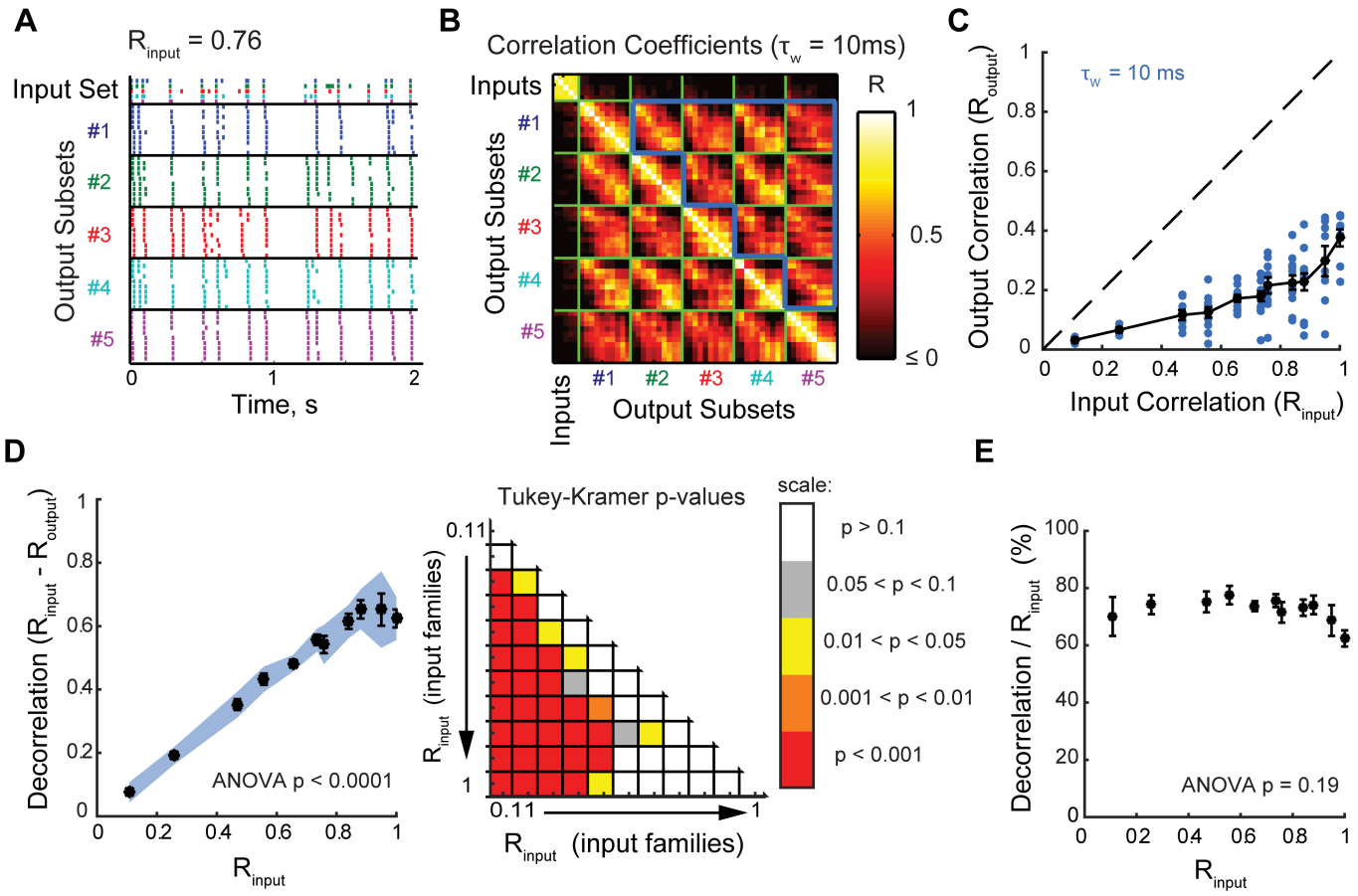
A
R_input = 0.76
Input Set
Output Subsets
#1
#2
#3
#4
#5
0
1
2
Time, s
B
Correlation Coefficients (τ_w = 10ms)
Inputs
Output Subsets
R
1
0.5
≤ 0
#1 #2 #3 #4 #5
Inputs
Output Subsets
C
τ_w = 10 ms
Output Correlation (R_output)
Input Correlation (R_input)
D
Decorrelation (R_input - R_output)
ANOVA p < 0.0001
R_input
Tukey-Kramer p-values
0.11
R_input (input families)
R_input (input families)
scale:
p > 0.1
0.05 < p < 0.1
0.01 < p < 0.05
0.001 < p < 0.01
p < 0.001
E
Decorrelation / R_input (%)
ANOVA p = 0.19
R_input

Figure 2

Figure 2. Input spiketrains are decorrelated at the level of individual granule cells.

(A) Example of a recording set (input set + output set): the raster plot shows one set of input spiketrains and the children output spiketrains recorded from one GC, organized so that output subsets (i.e., the ten children coming from one parent input spiketrain) are together and of the same color.

(B) Corresponding 55x55 correlation coefficient matrix using a binning window (τ_w) of 10 ms. Each small square represents the correlation coefficient between two spiketrains. R_{output} is defined as the mean of correlations between individual output spiketrains driven by different input spiketrains, as outlined by the bold blue border, which excludes comparisons between outputs generated from the same parent input.

(C) For each of the 102 recording sets (blue dots), R_{output} was lower than $R_{input.}$

(D) *Left*: effective decorrelation averaged over all recording sets as a function of R_{input}. Although there is a significant decorrelation for all tested input sets (one-sample T-tests: the blue shade indicates the 95% confidence interval that average decorrelation is significantly above 0), they are effectively decorrelated to different magnitudes (one-way ANOVA, $p<0.0001$). *Right:* post-hoc Tukey-Kramer tests show that the decorrelation is significantly different (higher) for highly similar input spiketrains than for already dissimilar inputs.

(E) When the effective decorrelation is normalized to the correlation of the input set, there is no significant difference between input sets (ANOVA, $p = 0.18$).

In all graphs, $\tau_w = 10$ ms and black bars represent SEM.

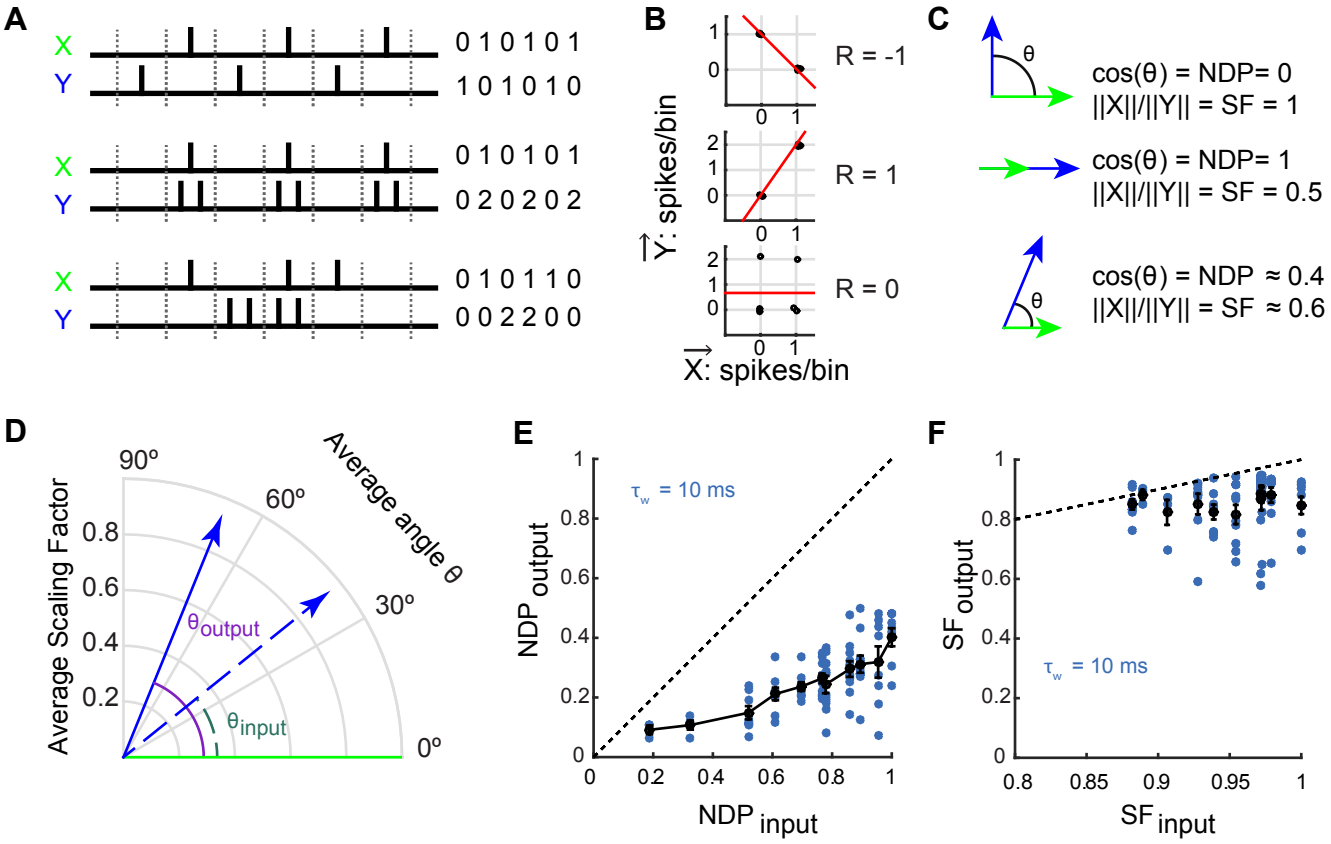
A
X
Y
0 1 0 1 0 1
1 0 1 0 1 0
0 1 0 1 0 1
0 2 0 2 0 2
0 1 0 1 1 0
0 0 2 2 0 0
B
R = -1
R = 1
R = 0
Y: spikes/bin
X: spikes/bin
C
cos(θ) = NDP= 0
||X||/||Y|| = SF = 1
cos(θ) = NDP= 1
||X||/||Y|| = SF = 0.5
cos(θ) = NDP ≈ 0.4
||X||/||Y|| = SF ≈ 0.6
D
Average Scaling Factor
Average angle θ
90º
60º
30º
0º
θoutput
θinput
E
τw = 10 ms
NDP output
NDP input
F
τw = 10 ms
SF output
SF input

Figure 3

Figure 3. Orthogonalization of input spiketrains is a strong component of temporal pattern separation by single granule cells.

(A-C) Three hypothetical cases of pairs of spiketrains and their associated correlation coefficients (R), normalized dot products (NDP) and scaling factors (SF), showing that the three metrics are not equivalent.

(A) Synthetic spiketrains (X and Y pairs) divided into six bins, with the corresponding number of spikes per bin.

(B) R between each pair of X and Y describes the linear regression between the number of spikes in the bins of X versus the corresponding bins in Y (jitter was added to make all points visible).

(C) Geometric view of vectors X and Y, where each bin is a dimension of a 6-dimensional space, and the number of spikes in a bin is the coordinate along this dimension. NDP measures how close to orthogonal two spiketrains are and SF measures how different their binwise firing rates are.

(D) Vector representation of experimental data from one recording set, showing the average similarity between a set of input spiketrains (dashed line and green angle, $R_{input} = 0.76$) and the average similarity between the fifty corresponding output spiketrains (solid line, purple angle, over the same subsets as enclosed in the blue border in **Figure 2B**). The angles are derived from the NDP whereas the lengths of each vector express differences in binwise firing rates (SF). Here, outputs are more orthogonal (closer to 90˚) than their inputs with little difference in scaling.

(E-F) NDP_{output} or SF_{output} as a function of NDP_{input} or SF_{input}. Mean and SEM in black.

(E) All data points (102 recording sets) are below the dashed identity line indicating that outputs are closer to orthogonality (NDP = 0) than their respective inputs. The average orthogonalization (NDP_{input}-NDP_{output}) is significant for all input sets (one-sample T-tests, $p < 0.05$).

(F) Most points fall slightly below the dashed identity line, suggesting that pattern separation by scaling of the binwise firing rate is present but weak at τ_w = 10ms. The average scaling (SF_{input}-SF_{output}) is significant for all input sets except the three most dissimilar (SF_{input} = 0.88, 0.89, 0.90) (one-sample T-tests, $p < 0.05$).

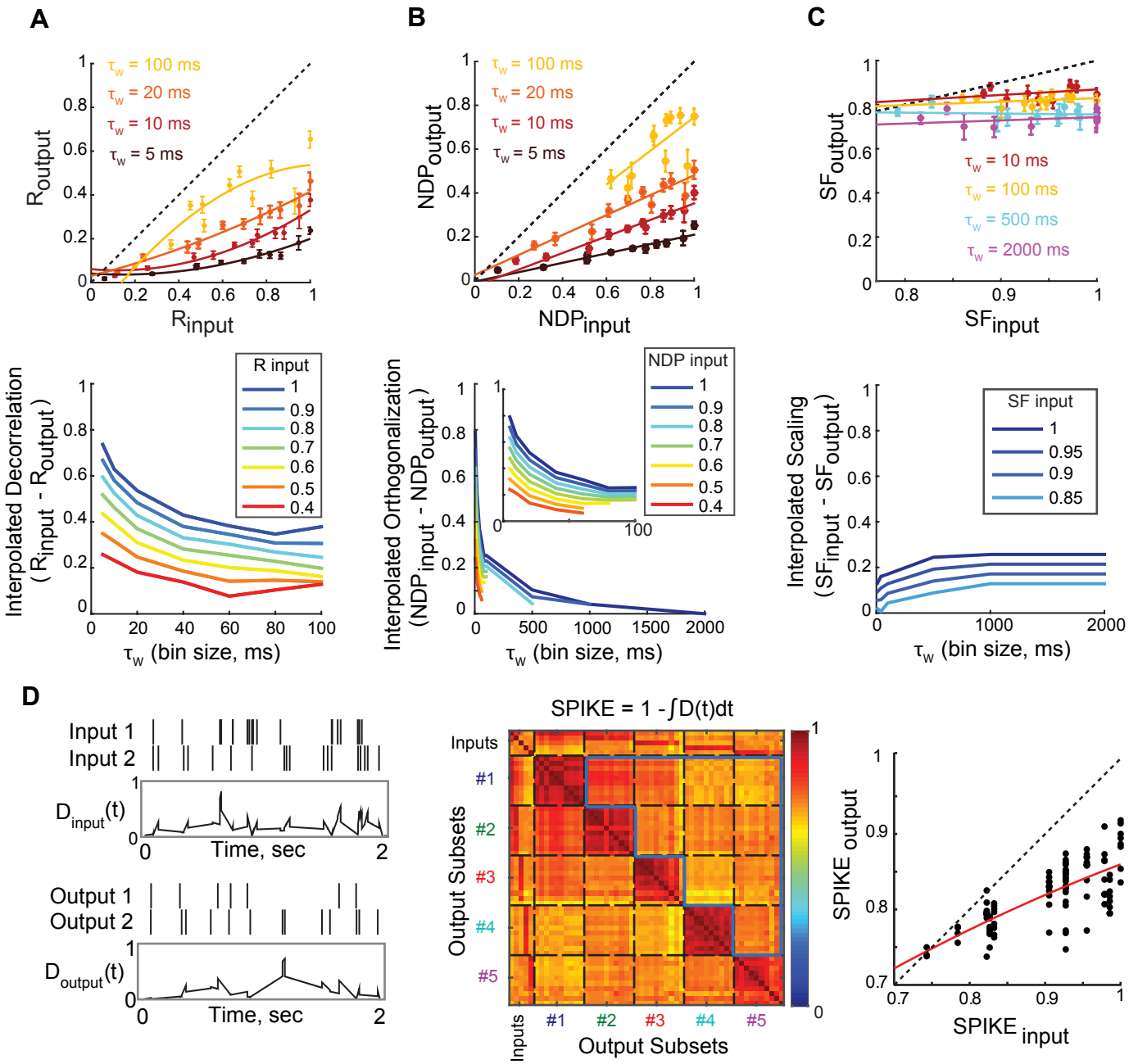
A
B
C
D
τw = 100 ms
τw = 20 ms
τw = 10 ms
τw = 5 ms
Routput
Rinput
NDPoutput
NDPinput
τw = 10 ms
τw = 100 ms
τw = 500 ms
τw = 2000 ms
SFoutput
SFinput
R input
1
0.9
0.8
0.7
0.6
0.5
0.4
Interpolated Decorrelation
(Rinput - Routput)
τw (bin size, ms)
NDP input
Interpolated Orthogonalization
(NDPinput - NDPoutput)
SF input
1
0.95
0.9
0.85
Interpolated Scaling
(SFinput - SFoutput)
Input 1
Input 2
Dinput(t)
Time, sec
Output 1
Output 2
Doutput(t)
SPIKE = 1 - ∫D(t)dt
Inputs
#1
#2
#3
#4
#5
Output Subsets
SPIKE output
SPIKE input

Figure 4

Figure 4. Single granule cells perform pattern separation from millisecond to second timescales using different codes.

(A) *Top:* Average R_{output} as a function of R_{input}, measured with different time windows τ_w. Solid curves are fitted parabolae. Each color corresponds to a different τ_w ranging from 5 ms to 100 ms. B*ottom:* Effect of τ_w on the effective decorrelation, interpolated from the parabolic regressions.

(B) Same as A but using NDP and linear regressions. *Bottom:* Note that the timescale axis is extended to 2000 ms, with the inset showing an expansion over the shorter timescales).

(C) Same as B using SF.

(B-C) Note that as τ_w increases, pattern separation through orthogonalization becomes weaker but stronger through scaling.

(D) Similarity between spiketrains is here assessed with the binless SPIKE metric, directly using spike times. *Left:* example of two input spiketrains associated with two output spiketrains from a GC recording set, and the corresponding distances D(t) between spiketrains. D(t) can then be integrated over time to give a single value D. *Middle*: example of 55x55 matrix of SPIKE similarity (1-D) between all spiketrains of an example recording set. 0 means that spikes of two trains never happened close in time, and 1 that they were perfectly synchronous. The output SPIKE similarity ($SPIKE_{output}$) is defined the same way as for R, NDP or SF (average of the values inside the blue border). *Right*: $SPIKE_{output}$ of all GC recordings as a function of their input similarity ($SPIKE_{input}$), fitted with a parabola (red line). Most data points are below the dashed identity line indicating that output spiketrains are less similar than inputs. The average $SPIKE_{input}$-$SPIKE_{output}$ is significantly above 0 for all input sets except the two most dissimilar ($SPIKE_{input}$ = 0.74, 0.78) (one-sample T-tests, $p < 0.05$).

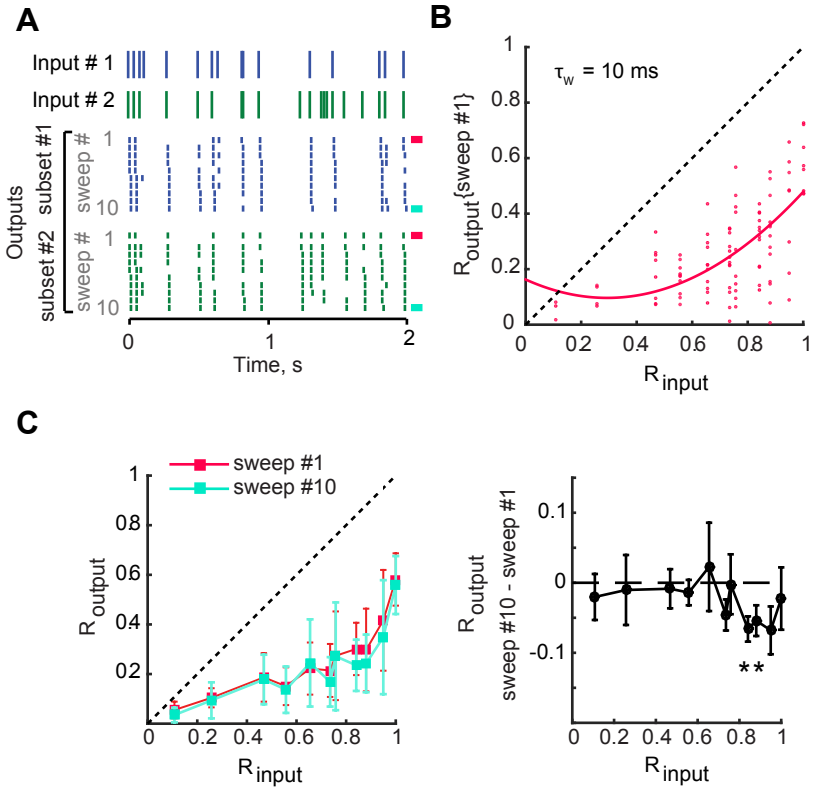
A
Input # 1
Input # 2
Outputs
subset #1
sweep #
1
10
subset #2
sweep #
1
10
0
1
2
Time, s
B
τw = 10 ms
Routput{sweep #1}
Rinput
C
sweep #1
sweep #10
Routput
Rinput
Routput
sweep #10 - sweep #1
**
Rinput

Figure 5

Figure 5. Input spiketrains are efficiently separated upon their first presentations.

(A) Two of five inputs are shown with corresponding output spiketrains. The first output sweep is marked with a pink box (right) and last sweep is marked with a blue box.

(B) R_{output}, computed from the first sweep of five output trains only (pink), as a function of R_{input}, fitted with a parabola. All data points are below the identity line indicating that outputs are effectively decorrelated compared to their inputs even when input patterns have only been presented once each. The average decorrelation (R_{input}-R_{output}) is significant for all input sets (one-sample T-tests, $p < 0.01$) except for $R_{input} = 0.11$ ($p = 0.1$).

(C) *Left*: Average output correlations between spiketrains of the first sweep (pink) and the last sweep (blue). There is no significant difference (F-test comparing the two distributions using parabolic regressions, $p = 0.47$. Error bars are SEM). *Right:* When taking into account that the two distributions are paired, we detect that a few output correlations are significantly lower for the last sweep than for the first one (one-sample T-test on the difference between R_{output} of the first and last sweep of each recording set, asterisks signify $p < 0.05$). This is evidence, though weak, that repetition of input spiketrains might improve pattern separation for highly similar inputs.

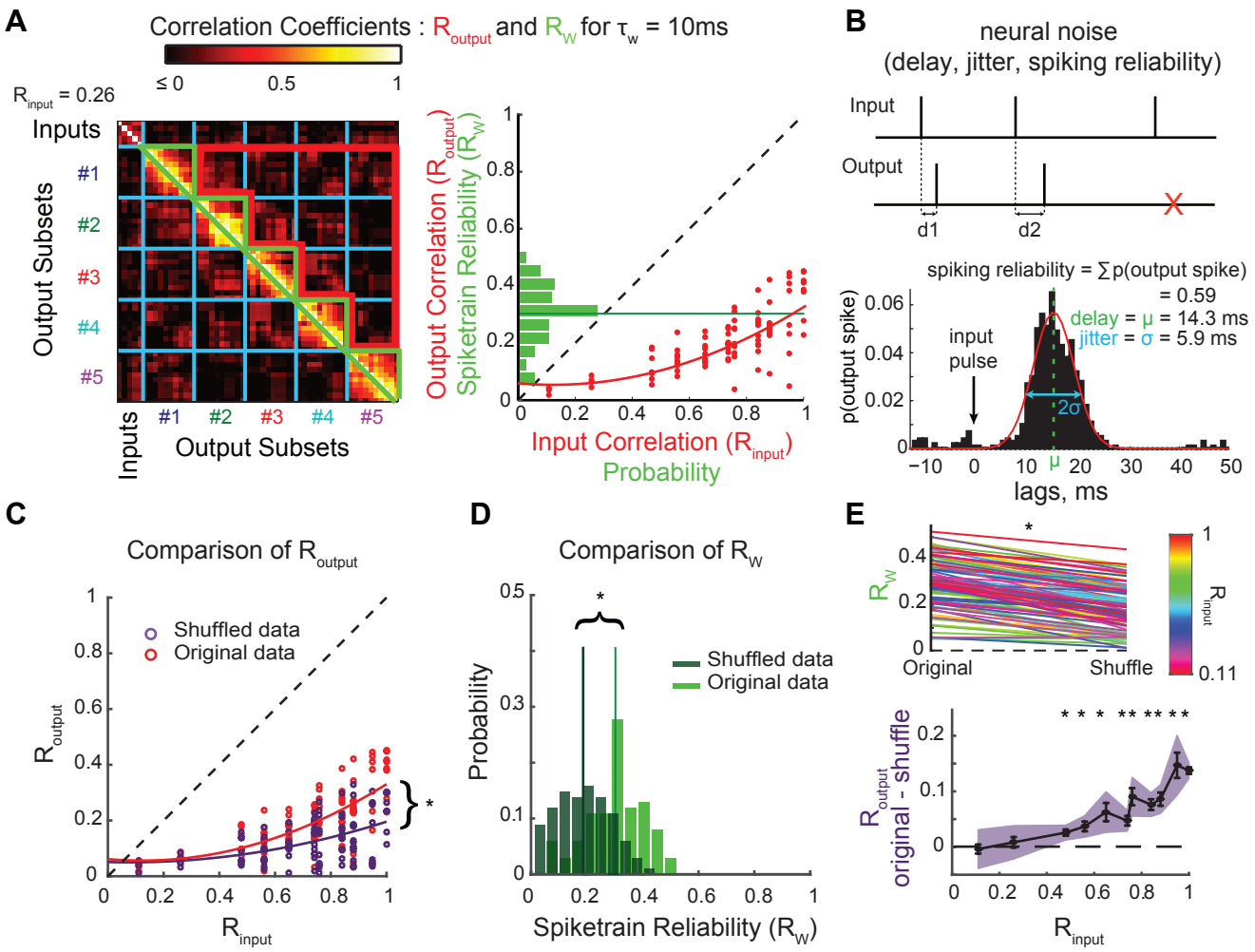
A
Correlation Coefficients : R_output and R_W for τ_w = 10ms
≤ 0
0.5
1
R_input = 0.26
Inputs
Output Subsets
#1
#2
#3
#4
#5
Output Correlation (R_output)
Spiketrain Reliability (R_W)
Input Correlation (R_input)
Probability
B
neural noise
(delay, jitter, spiking reliability)
Input
Output
d1
d2
spiking reliability = ∑p(output spike)
= 0.59
delay = μ = 14.3 ms
jitter = σ = 5.9 ms
input
pulse
2σ
p(output spike)
lags, ms
C
Comparison of R_output
Shuffled data
Original data
R_output
R_input
D
Comparison of R_W
Shuffled data
Original data
Probability
Spiketrain Reliability (R_W)
E
R_W
Original
Shuffle
R_input
R_output original - shuffle
R_input

Figure 6

Figure 6. Pattern separation in single GCs is not explained by neural noise.

(A) The variability of output spiketrains in response to the same input train sets the upper bound for R_{output}. *Left:* Correlations between pairs of output spiketrains associated with different input trains (enclosed by red, R_{output}) and pairs of different output spiketrains associated with the same input train (enclosed by green, R_w: spiketrain reliability, the reproducibility of the output given the same input). *Right:* Empirical probability distribution of R_w for all recordings (dark green line is the mean: $\langle R_w \rangle = 0.3$), overlaid on the distribution of R_{output} as a function of R_{input} (102 recording sets) fitted with a parabola. Note that means $\langle R_w \rangle$ and $\langle R_{output} \rangle$ for $R_{input} = 1$ are close because they both assess the reproducibility of the output when the input is the same.

(B) Characterization of neural noise. *Top:* example of input and output spiketrains illustrating variable delay of the response spike after an input spike (d1<d2) or failure to spike after an input spike (red cross). *Bottom*: Example from one GC recording. The spike-wise noise in output spiketrains is characterized by the average spike delay, the standard deviation of this delay (jitter) and the probability of spiking after an input spike (spiking reliability of the cell, SR).

(C-D) Effect of random shuffling on R_{output} and R_w.

(C) Patterns are *less* separated for GC than for random shuffling (F-test using parabolic regressions: $p < 0.0001$). (D) GC output is *more* reliable than for random shuffling (unpaired T-test, $p < 0.0001$; mean <Rw>{shuffle} = 0.19).

(E) Paired statistical tests show that shuffling leads to smaller R_{output} and R_w than original recordings. *Top:* paired T-test on all recording sets, $p < 0.0001$. *Bottom*: one-sample T-test on difference between shuffled and original data R_{output} performed on each R_{input} group. Black symbols correspond to the means, bars to SEM. The purple shade indicates the 95% confidence interval. Asterisks signify $p < 0.001$.

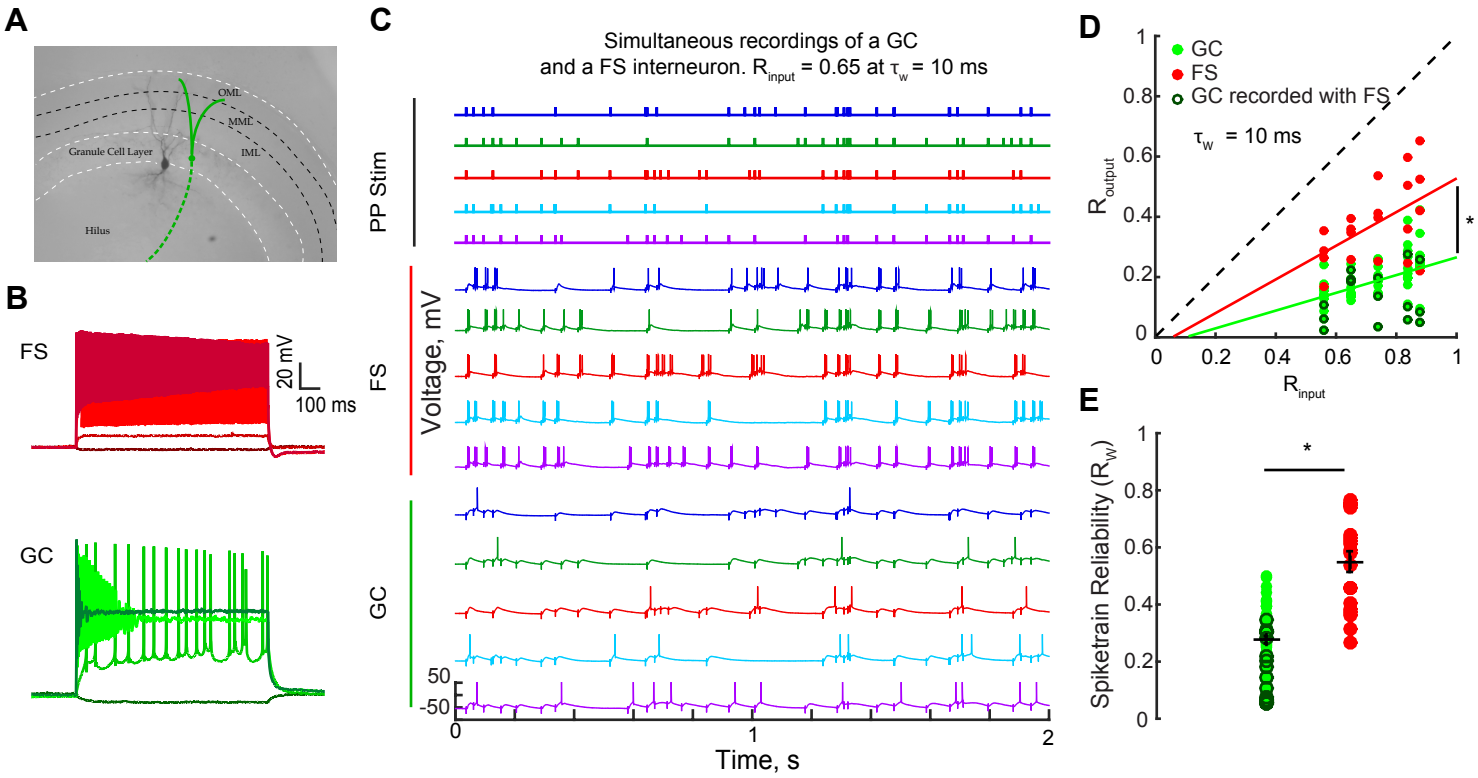
A
OML
MML
IML
Granule Cell Layer
Hilus
B
FS
20 mV
100 ms
GC
C
Simultaneous recordings of a GC
and a FS interneuron. R_{input} = 0.65 at τ_w = 10 ms
PP Stim
FS
GC
Voltage, mV
50
-50
0
1
2
Time, s
D
GC
FS
GC recorded with FS
τ_w = 10 ms
R_{output}
R_{input}
*
E
Spiketrain Reliability (R_W)
*

Figure 7

Figure 7. Fast-spiking interneurons of the DG perform lower levels of pattern separation than GCs.

(A) Picture of a recorded FS filled with biocytin (black). In the case of simultaneous recordings, the recorded GCs were close to the FS, as depicted by the schematic in green.

(B-C) Example of a simultaneous whole-cell recording of a GC and a neighboring FS.

(B) Simultaneous membrane potential recordings (baseline around -60mV) of a FS and a GC to the same set of current steps (-25pA, 100pA, 500pA and 1000pA).

(C) Simultaneous current-clamp recordings of the same FS and GC as in A in response to the five input traces of an input set with $R_{input} = 0.65$ (first sweep of five output trains). Simultaneous input and output trains have the same color.

(D) R_{output} versus R_{input} at $\tau_w = 10$ms. Data points correspond to recording sets: 20 for FS (red), and 61 for GC (green, with a darker shade open circle when simultaneously recorded with a FS). All GC recordings done at the same input correlations as FS recordings were used for an unpaired comparison: R_{output} distribution for FS is significantly higher in FS than in GC (F-test using linear regressions: $p < 0.0001$; unbalanced two-way ANOVA, stimulation groups: $p = 0.0015$, cell-types: $p < 0.0001$, interaction: $p = 0.72$.) Post-hoc Tukey-Kramer tests: significant difference for stimulation groups with measured correlation $R_{input} = 0.88$, 0.84 and 0.74 ($p < 0.01$).

(E) Spiketrain reliability R_W. Same color code and recording sets as in D**.** Unpaired T-test, $p < 0.0001$. (D-E) Note that when comparing only the simultaneous GC and FS recordings, we found similarly significant difference, both for R_{output} and R_w (see statistics table in **methods**). Asterisks signify $p < 0.0001$

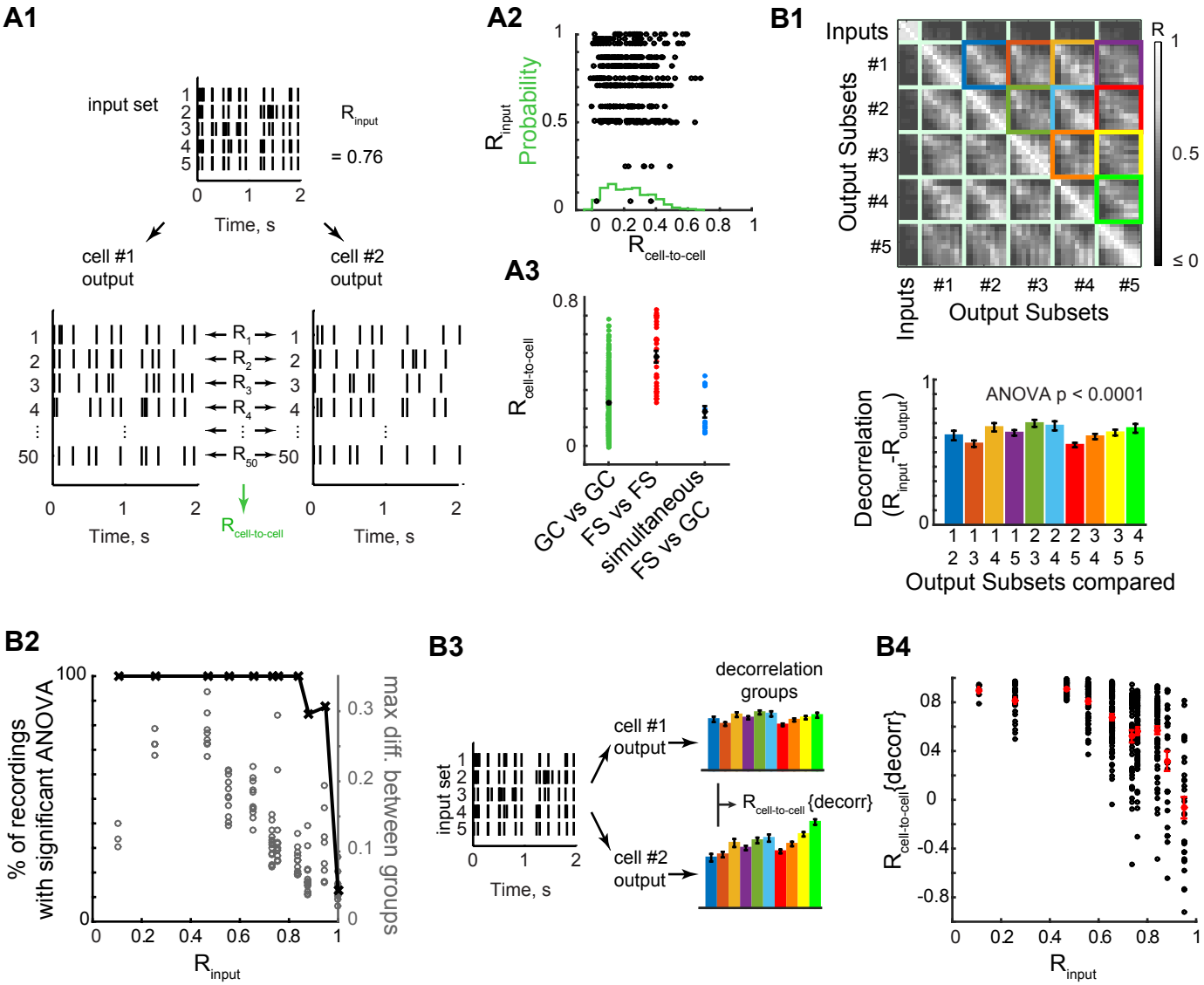
A1
input set
R_{input}
= 0.76
Time, s
cell #1 output
cell #2 output
R_1
R_2
R_3
R_4
R_{50}
$R_{cell-to-cell}$
A2
R_{input}
Probability
$R_{cell-to-cell}$
A3
$R_{cell-to-cell}$
GC vs GC
FS vs FS
simultaneous
FS vs GC
B1
Inputs
Output Subsets
R
≤ 0
Decorrelation (R_{input}-R_{output})
ANOVA p < 0.0001
Output Subsets compared
B2
% of recordings with significant ANOVA
max diff. between groups
R_{input}
B3
input set
decorrelation groups
cell #1 output
cell #2 output
$R_{cell-to-cell}${decorr}
B4
$R_{cell-to-cell}${decorr}
R_{input}

Figure 8

Figure 8. Cell-to-cell comparisons show that granule cells have variable responses to identical inputs and perform pattern separation in different ways.

(A) Spiketrain-wise comparison between recording sets.

(A1) The similarity between pairs of spiketrains coming from two different output sets but associated to the same input set and with the same sweep number is assessed with the Pearson's correlation coefficient (τ_w = 10 ms). The fifty resulting coefficients are then averaged to give $R_{cell\text{-}to\text{-}cell}$, a single number measuring the overall similarity of output spiketrains between two recording sets. All combinations of pairs of output sets from the same input set were compared.

(A2) Probability distribution of $R_{cell\text{-}to\text{-}cell}$ (green line) across all GC recordings. The distribution of $R_{cell\text{-}to\text{-}cell}$ (black circles) is not dependent on R_{input}.

(A3) Distribution of $R_{cell\text{-}to\text{-}cell}$ for different cell-types. (GC to GC: n = 470 , FS to FS: n = 30, FS to GC simultaneously recorded: n = 15).

(B) Comparison of the pattern separation levels between recording sets.

(B1) Top: same as Fig. 2B but in grey scale. Colored squares enclose the coefficients comparing outputs in response to two different input trains which have a R_{input} ~ 0.76 shown in (A1). Bottom: Average decorrelation of input spiketrains for each group of comparisons enclosed by the matching colored square above. Here, for each of these groups, R_{output} is the average of the coefficients in the square of the corresponding color and R_{input} is the correlation coefficient between the corresponding two parent input trains (not the average R over all input trains). For each recording set, a one-way ANOVA was performed to compare the 10 groups. For the GC shown, the ANOVA was significant, suggesting that levels of decorrelation depend on the identity of the input trains.

(B2) Percentage of recording sets with a significant ANOVA (crosses in black, axis on left). For all input sets except $R_{input} = 1$ the proportion was high. The distribution of the largest difference between the mean of the ten decorrelation groups of a single recording set is also plotted (grey circles, axis on right).

(B3) To assess whether cells perform similar levels of pattern separation we computed $R_{cell\text{-}to\text{-}cell}\{decorr\}$, the Pearson's correlation coefficient between decorrelation groups (as in B1) from pairs of recording sets.

(B4) Distribution of $R_{cell\text{-}to\text{-}cell}\{decorr\}$ (GCs only, mean and SEM in red). Like in **A**, all combinations of pairs from the same input set were compared (442 total comparisons). $R_{input} = 1$ was excluded. This analysis shows that, in our experimental conditions, not all GC decorrelate input spiketrains the same way.

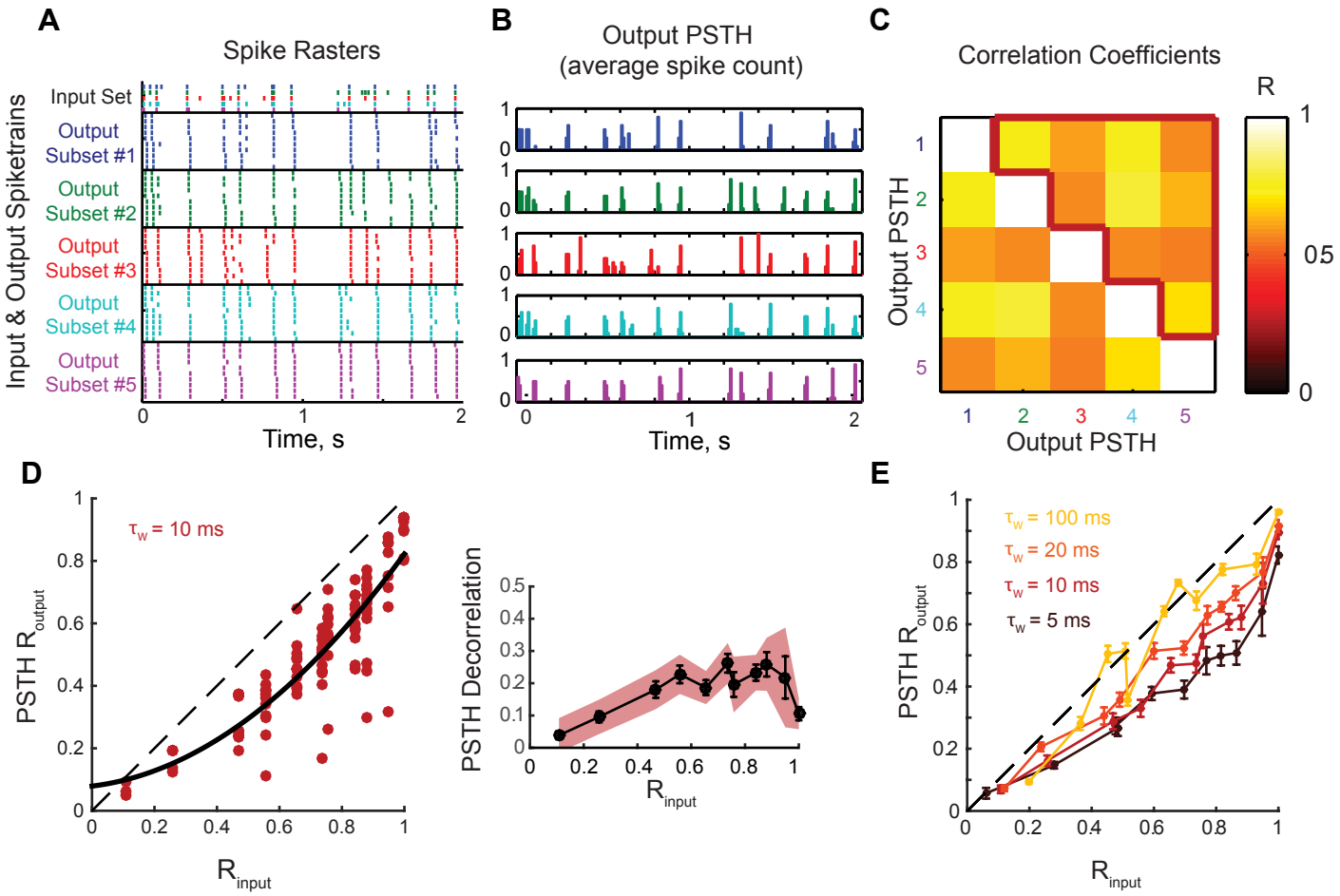
A
Spike Rasters
Input & Output Spiketrains
Input Set
Output Subset #1
Output Subset #2
Output Subset #3
Output Subset #4
Output Subset #5
Time, s
B
Output PSTH (average spike count)
Time, s
C
Correlation Coefficients
R
Output PSTH
Output PSTH
D
τ_w = 10 ms
PSTH R_{output}
R_{input}
PSTH Decorrelation
R_{input}
E
τ_w = 100 ms
τ_w = 20 ms
τ_w = 10 ms
τ_w = 5 ms
PSTH R_{output}
R_{input}

Figure S1

Figure S1 related to Figure 1 and Figure 6. Decorrelation of input patterns measured from PSTHs of single granule cell recordings.

(A) Example of a recording set with an average R_{input} = 0.76 (same as in **Figure 2A**).

(B) The ten children output spiketrains of each of the five inputs can be averaged to give the five output peristimulus histograms (PSTH) corresponding to the five input trains. The 10 ms binned PSTHs of the output rasters in A are shown.

(C) Correlation coefficients between all pairs of the five output PSTHs. The mean correlation (PSTH R_{output}) is the average of coefficients inside the red border, and excludes self-comparisons.

(D) *Left:* PSTH R_{output} as a function of R_{input} (102 recording sets, in red), fitted with a parabola (black). All points are below the identity line indicating decorrelation of outputs compared to inputs. *Right:* Average effective decorrelation (R_{input} – PSTH R_{output}) as a function of R_{input} (bars are SEM) reveals a significant decorrelation for all input sets except for the most dissimilar (one-sample T-tests; shaded area is the 95% confidence interval for significant decorrelation). (E) Averaged PSTH R_{output} as a function of R_{input}, for different binning windows τ_w.

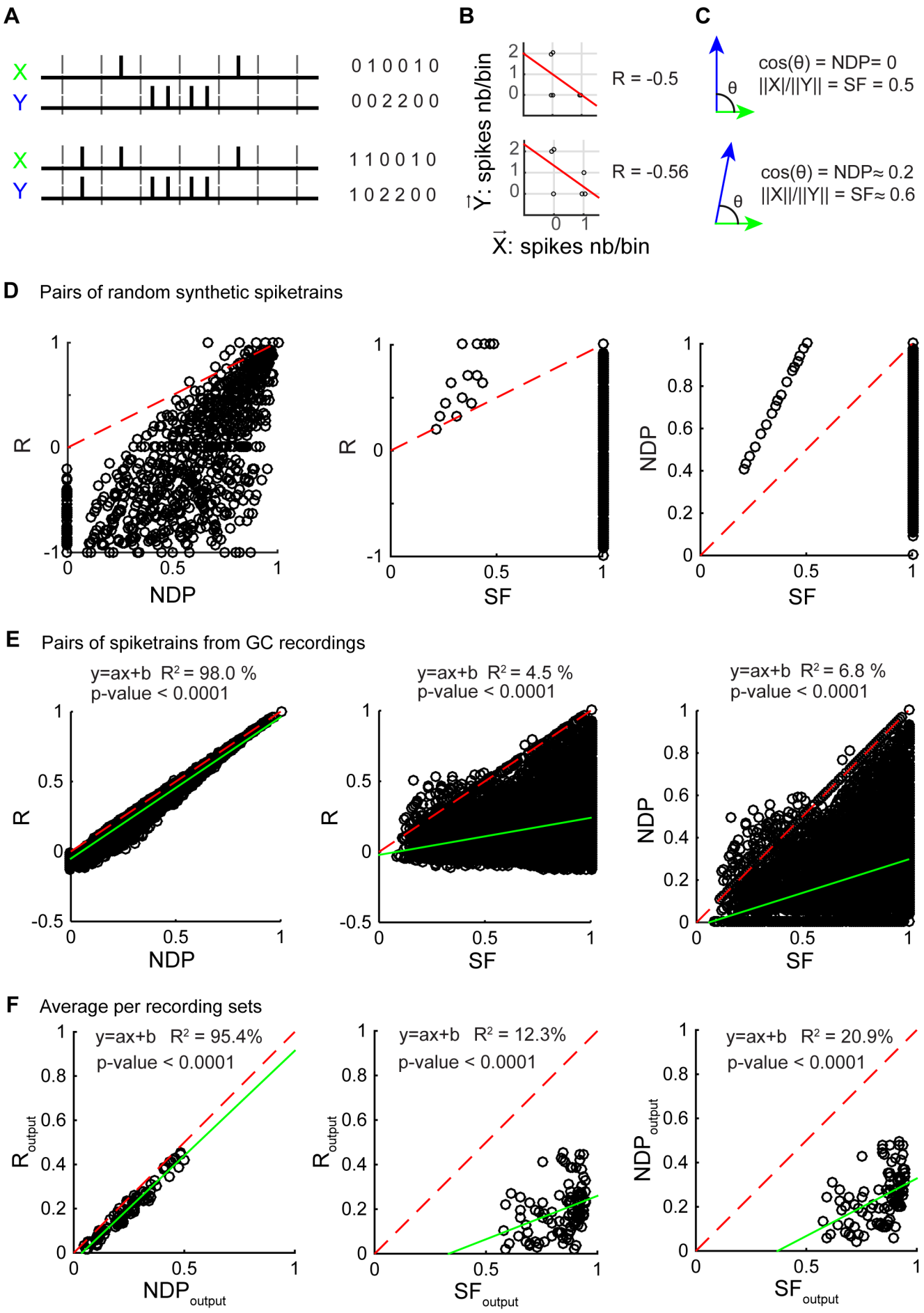
A
X
Y
0 1 0 0 1 0
0 0 2 2 0 0
X
Y
1 1 0 0 1 0
1 0 2 2 0 0
B
R = -0.5
R = -0.56
Y: spikes nb/bin
X: spikes nb/bin
C
cos(θ) = NDP= 0
||X||/||Y|| = SF = 0.5
cos(θ) = NDP≈ 0.2
||X||/||Y|| = SF≈ 0.6
θ
D Pairs of random synthetic spiketrains
R
NDP
SF
E Pairs of spiketrains from GC recordings
y=ax+b R² = 98.0 %
p-value < 0.0001
y=ax+b R² = 4.5 %
p-value < 0.0001
y=ax+b R² = 6.8 %
p-value < 0.0001
F Average per recording sets
y=ax+b R² = 95.4%
p-value < 0.0001
y=ax+b R² = 12.3%
p-value < 0.0001
y=ax+b R² = 20.9%
p-value < 0.0001
R output
NDP output
SF output

Figure S2

Figure S2 related to Figure 3. The correlation coefficient, normalized dot product and scaling factor between spiketrains do not have a simple relationship.

(A-C) Two additional examples of hypothetical pairs (X and Y) of spiketrains divided into 6 bins, the number of spikes per bin constituting the numerical vector next to them (A right). The similarity between X and Y can be assessed by (B) the Pearson's correlation coefficient R describing the linear relationship between the number of spikes in corresponding bins or (C) by a vector analysis in a 6-dimensional space giving the angle between the vectors X and Y (computed from the normalized dot product, NDP) as well as the scaling factor (SF) between their norms. These examples provide the intuition that orthogonal vectors (NDP = 0) necessarily correspond to a negative correlation between the spiketrains but that anticorrelated spiketrains (R<0) are not necessarily orthogonal. Also, SF gives information about the firing rate per bin that R doesn't necessarily take into account (see second example in **Figure 3**).

(D) Relationships between these 3 similarity metrics (R, NDP and SF) computed between 1,000 randomly generated spiketrains with six bins like in (A) (All pairs combinations = 499,500 data points). For simplicity, each bin can only take a value between 0 and 2, which is why points in the SF graph are less distributed.

(E) Relationships between these three similarity metrics for 102 experimental GC recording sets. (124,950 data points)

(F) Relationship between these three similarity metrics averaged for each GC recording set (102 data points).

(E-F) Green lines correspond to a linear regression, the R^2 and the p-value of which are indicated in each panel. Note that although R and NDP are well correlated in our experimental data

(R^2>0.95) (E-F left), there is not a linear relationship between R and NDP in theory **(**D left and see **methods**).

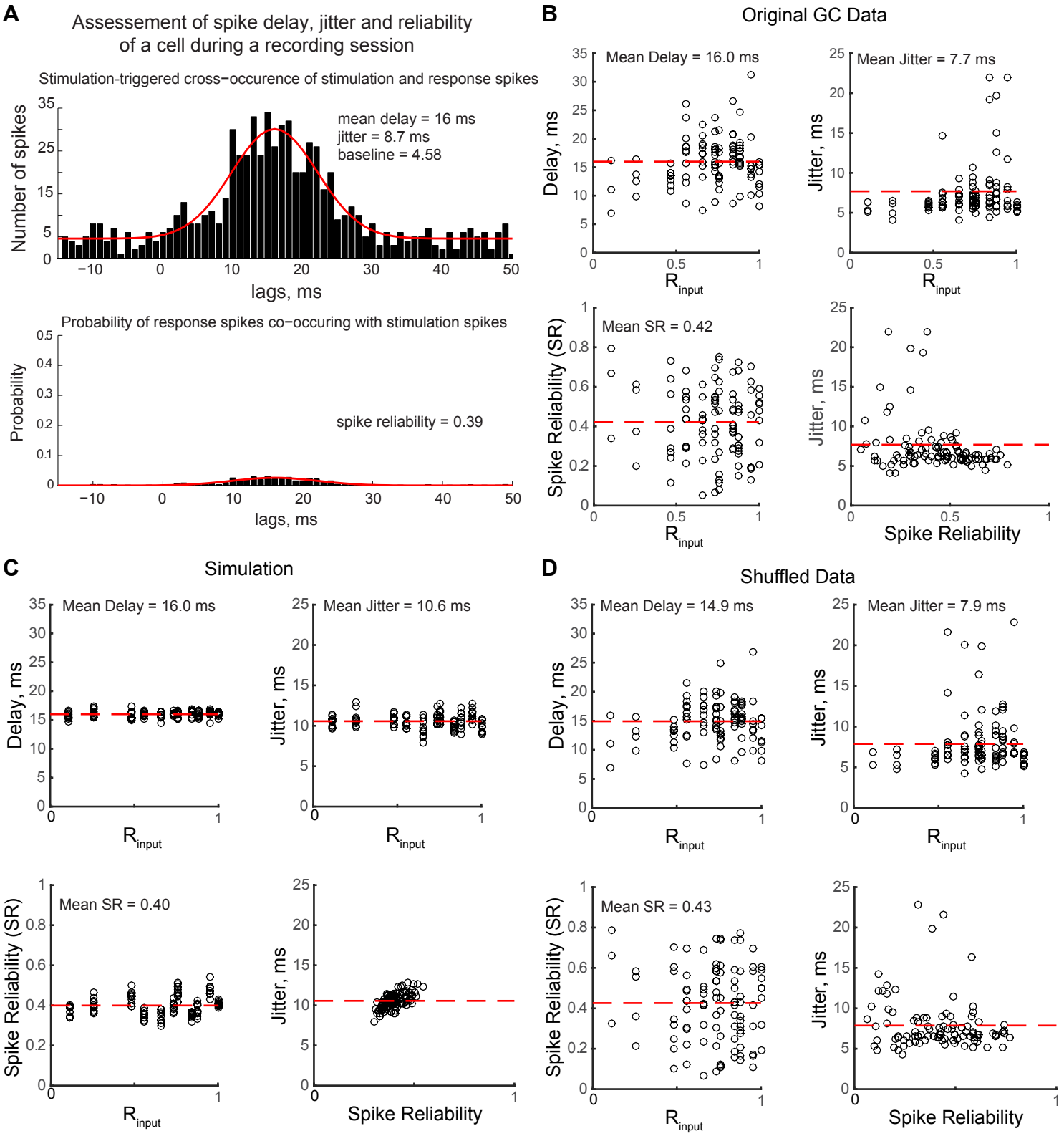
A
Assessement of spike delay, jitter and reliability
of a cell during a recording session
Stimulation-triggered cross−occurence of stimulation and response spikes
Number of spikes
mean delay = 16 ms
jitter = 8.7 ms
baseline = 4.58
lags, ms
Probability of response spikes co−occuring with stimulation spikes
Probability
spike reliability = 0.39
lags, ms
B
Original GC Data
Mean Delay = 16.0 ms
Delay, ms
Mean Jitter = 7.7 ms
Jitter, ms
Mean SR = 0.42
Spike Reliability (SR)
Jitter, ms
Spike Reliability
C
Simulation
Mean Delay = 16.0 ms
Delay, ms
Mean Jitter = 10.6 ms
Jitter, ms
Mean SR = 0.40
Spike Reliability (SR)
Jitter, ms
Spike Reliability
D
Shuffled Data
Mean Delay = 14.9 ms
Delay, ms
Mean Jitter = 7.9 ms
Jitter, ms
Mean SR = 0.43
Spike Reliability (SR)
Jitter, ms
Spike Reliability

Figure S3

Figure S3 related to Figure 6. Spike delay, jitter and reliability distributions for real data, simulations and shuffled data

(A) Cross-occurrence method to measure spike delay, jitter and spiking reliability of a neuron during a given recording session. *Top*: Example histogram of output spikes occurring after input spikes, fitted (red curve) with a Gaussian distribution N(μ,σ, baseline), where μ is the mean delay and σ is the jitter of this delay. Lag 0 ms corresponds to the input spikes time. In this example, output spikes are generated on average 16ms after a stimulation impulse (delay) with a jitter (σ) of 8.7 ms. *Bottom***:** the baseline is subtracted and the histogram divided by the number of input spikes during the recording session. This gives the distribution of the probability of spiking after an input spike, the sum of probabilities defining the spiking reliability of the cell during the recording session. Here the neuron fires 39 % of the time after an input spike.

(B-D) Delay, jitter and spiking reliability (SR) distributions for (B) the original recordings, (C) the simulations and (D) the shuffled data set. Dashed horizontal red lines are means.

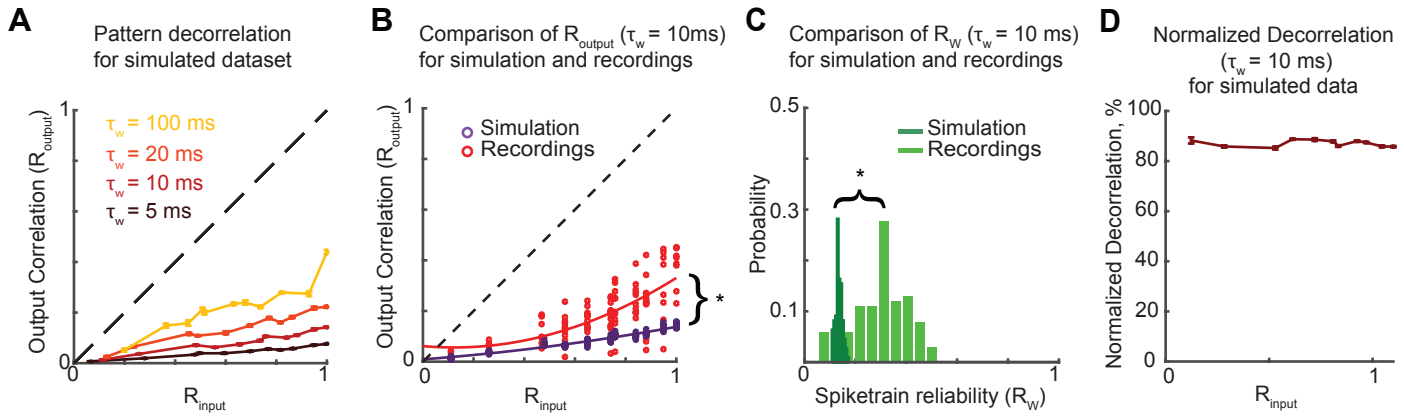
A
Pattern decorrelation
for simulated dataset
Output Correlation (R_{output})
τ_w = 100 ms
τ_w = 20 ms
τ_w = 10 ms
τ_w = 5 ms
R_{input}
B
Comparison of R_{output} (τ_w = 10ms)
for simulation and recordings
Simulation
Recordings
*
C
Comparison of R_W (τ_w = 10 ms)
for simulation and recordings
Probability
Simulation
Recordings
Spiketrain reliability (R_W)
D
Normalized Decorrelation
(τ_w = 10 ms)
for simulated data
Normalized Decorrelation, %

Figure S4

Figure S4 related to Figure 6. Simulation of purely noisy outputs significantly decreases R_{output} and spiketrain reliability

Simulations of output spiketrains to the different input sets with random spiking following a Gaussian distribution defined by the mean spike delay, mean jitter and mean reliability of the original recordings.

(A) Pattern separation for different time windows τ_w (dots: average R_{output} across all simulated "recordings" for a given input set, bars are SEM).

(B) R_{output} distribution at $\tau_W = 10$ ms, for simulated data and original data. Distributions are fitted with parabolae and significantly different (F-test using parabolic regressions: $p < 0.0001$).

(C) R_w distributions are significantly different (unpaired T-test, $p < 0.0001$; <Rw>{simul} = 0.14).

(D) Like in the original data (**Figure 2E**), the average normalized decorrelation ((R_{input}-R_{output})/R_{input}) seems invariant. Bars are SEM.

(C-D) Asterisks signify statistical significance

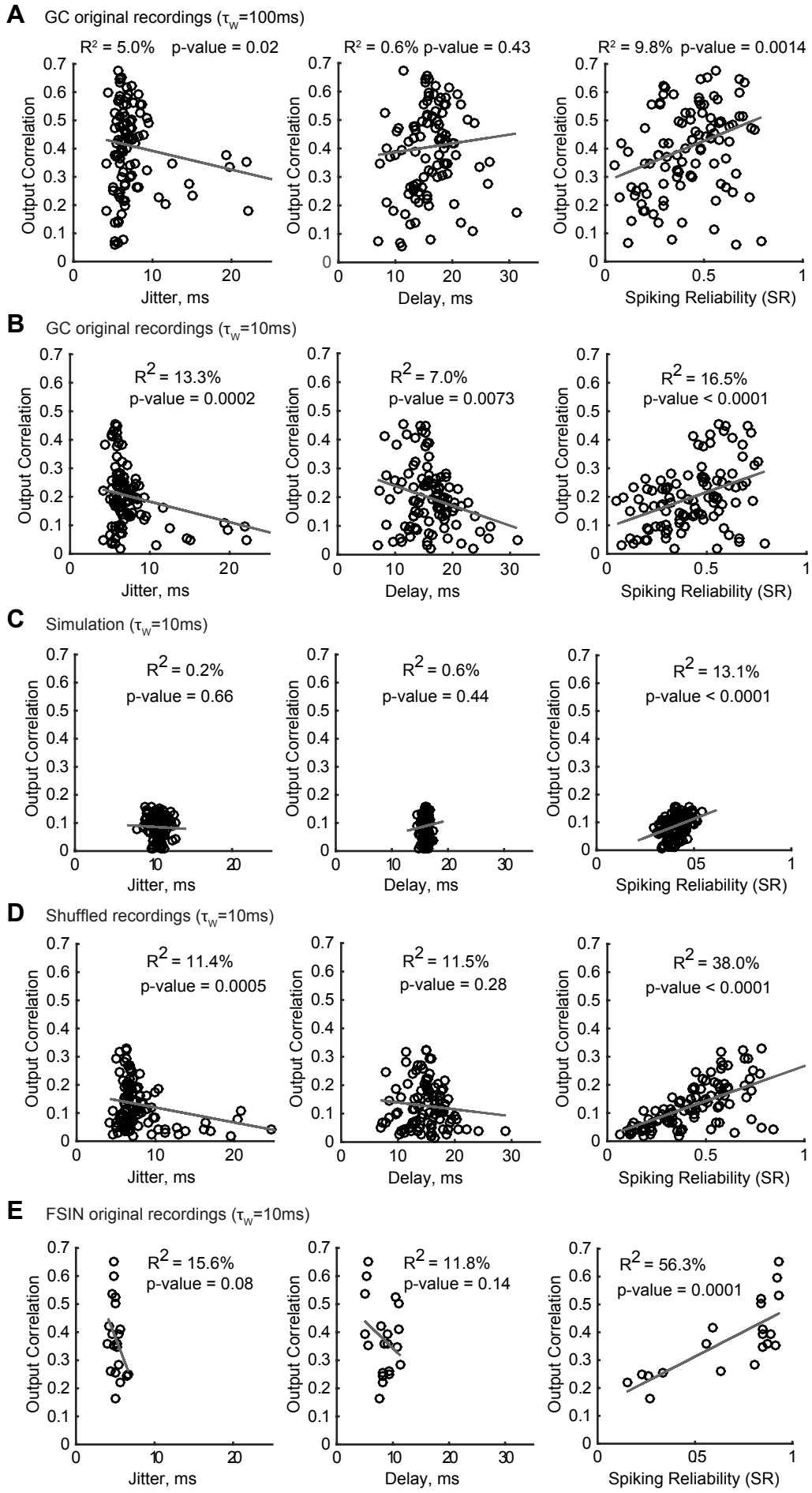
A
GC original recordings (τ_W=100ms)
R^2 = 5.0% p-value = 0.02
R^2 = 0.6% p-value = 0.43
R^2 = 9.8% p-value = 0.0014
B
GC original recordings (τ_W=10ms)
R^2 = 13.3%
p-value = 0.0002
R^2 = 7.0%
p-value = 0.0073
R^2 = 16.5%
p-value < 0.0001
C
Simulation (τ_W=10ms)
R^2 = 0.2%
p-value = 0.66
R^2 = 0.6%
p-value = 0.44
R^2 = 13.1%
p-value < 0.0001
D
Shuffled recordings (τ_W=10ms)
R^2 = 11.4%
p-value = 0.0005
R^2 = 11.5%
p-value = 0.28
R^2 = 38.0%
p-value < 0.0001
E
FSIN original recordings (τ_W=10ms)
R^2 = 15.6%
p-value = 0.08
R^2 = 11.8%
p-value = 0.14
R^2 = 56.3%
p-value = 0.0001
Output Correlation
Jitter, ms
Delay, ms
Spiking Reliability (SR)

Figure S5

Figure S5 related to Figure 6 and Figure 7. Relationship between R_{output} and noise characteristics for various conditions and cell-types.

Plots of the average output correlation (R_{output}) of each recording set: 102 for GC **(A-D)**, 20 for FSIN **(E)**, as a function of noise characteristics (spike jitter, delay and reliability). Solid grey lines are the best linear fit, with R^2 and p-values noted in each panel. Correlations are poor (low R^2) for original GC recordings, regardless of the time window τ_w used to measure R_{output} **(A-B)**, suggesting that noise characteristics are not good predictors of R_{output} in actual experiments. This is in opposition to the shuffled GC recordings **(D)**, where the output is only governed by random processes: in this case, the spiking reliability (SR) is a good predictor of R_{output} **(D right)**. SR (computed from nbFS data) is an even stronger predictor of R_{output} in FS interneurons **(E right)**.

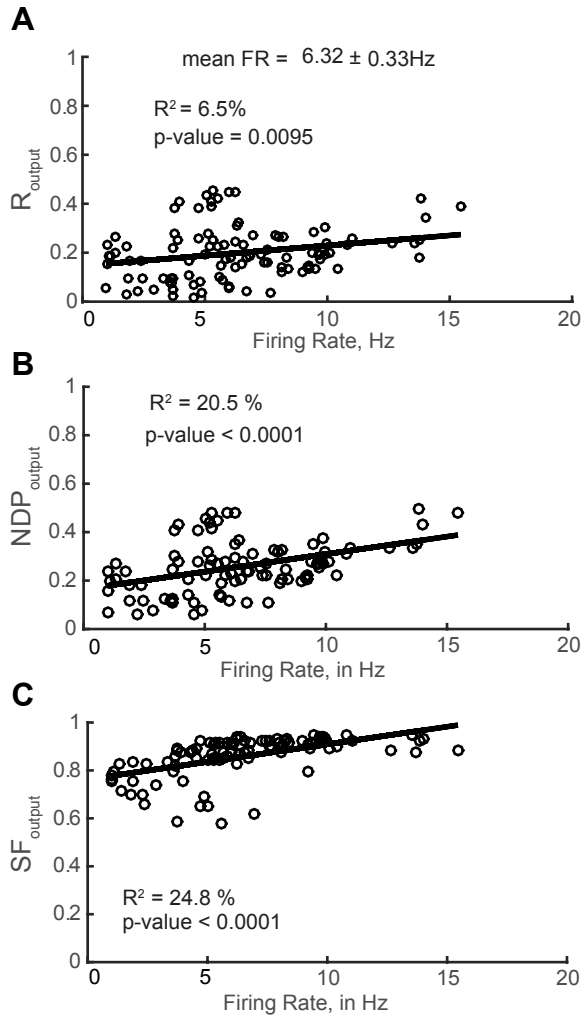
A
mean FR = 6.32 ± 0.33Hz
R² = 6.5%
p-value = 0.0095
R output
Firing Rate, Hz
B
R² = 20.5 %
p-value < 0.0001
NDP output
Firing Rate, in Hz
C
R² = 24.8 %
p-value < 0.0001
SF output
Firing Rate, in Hz

Figure S6

Figure S6 related to Figure 2, Figure 3 and Figure 6. The firing rate of individual recordings is not a good predictor of output correlation, normalized dot product or scaling factor of granule cells.

Data points correspond to the 102 recording sets in GCs. Solid black lines correspond to the best linear fit, with the associated R^2 and p-values noted in the panels. The output correlation **(A)**, NDP **(B)** and SF **(C)** were computed using a time window τ_w of 10 ms. The firing rate (FR) was computed for each recording set as the average FR of the 50 output spiketrains.

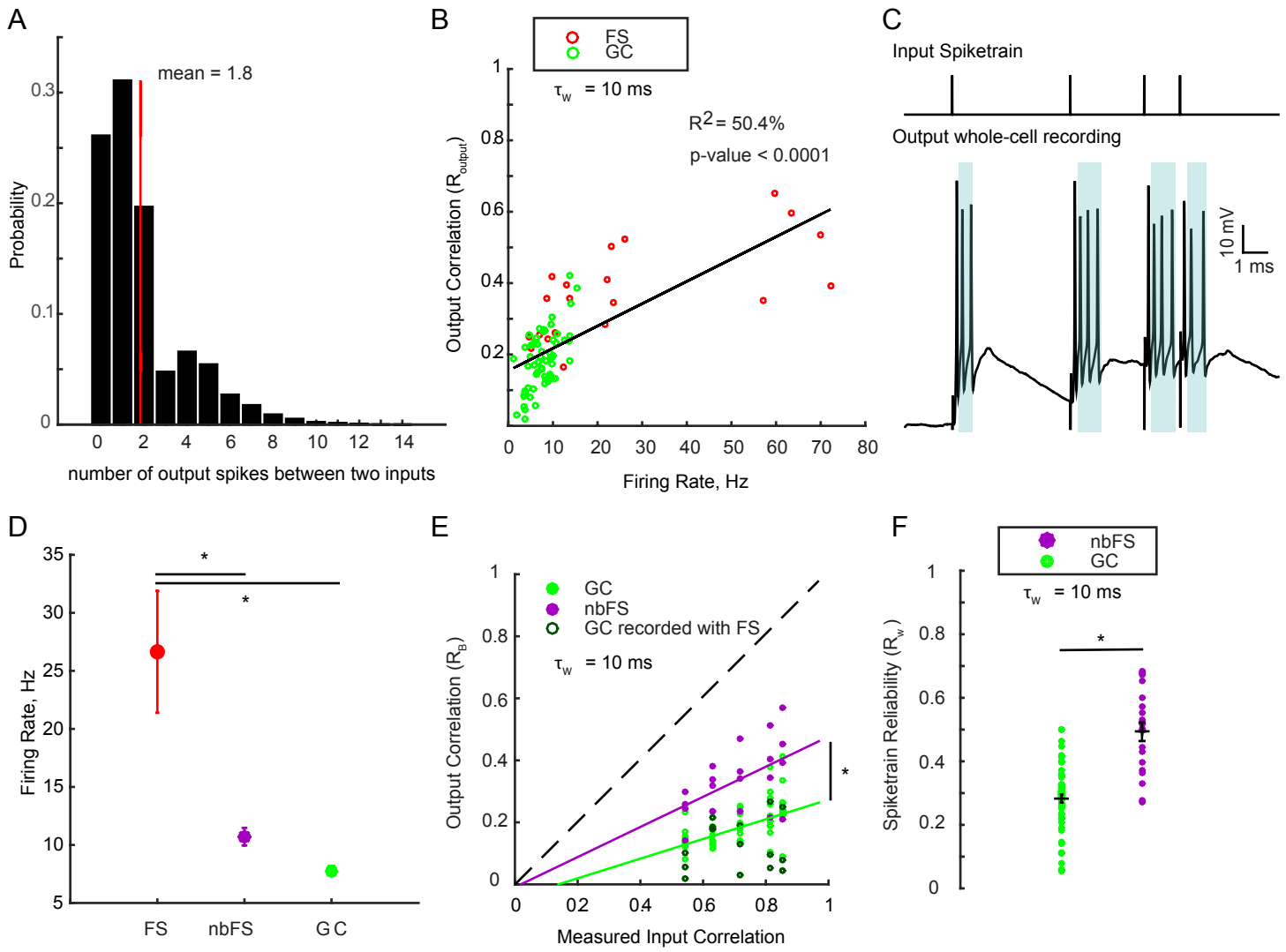
A
mean = 1.8
Probability
number of output spikes between two inputs
B
FS
GC
τ_w = 10 ms
R^2= 50.4%
p-value < 0.0001
Output Correlation (R_{output})
Firing Rate, Hz
C
Input Spiketrain
Output whole-cell recording
10 mV
1 ms
D
Firing Rate, Hz
FS
nbFS
GC
E
GC
nbFS
GC recorded with FS
τ_w = 10 ms
Output Correlation (R_B)
Measured Input Correlation
F
nbFS
GC
τ_w = 10 ms
Spiketrain Reliability (R_w)

Figure S7

Figure S7 related to Figure 7. Differences in pattern separation between FS and GC are not solely due to FS bursting behavior or higher firing rate.

(A) Probability of having 0, 1 or more output spikes between two input spikes assesses the bursting behavior in FS recordings.

(B) There is a strong correlation between the firing rate of a cell during the recording set for a given R_{input} and its R_{output} when we pool FS neurons with GCs. The linear regression, with R^2 and p-value in the panel, is to be compared with **Figure S6A** that shows a low correlation for GCs alone.

(C) Example of bursts in a FS (*Bottom*) in response to input spikes (*Top*). To assess the effect of bursting on R_{output}, we truncated each recorded spiketrain from FS neurons to keep only the first output spike between two input spikes, thus removing any burst without altering the SR of the cell. The blue shaded areas highlight the spikes that were removed. The resulting truncated dataset was termed "nbFS" for "non-burst FS".

(D) The firing rate of nbFS neurons is significantly reduced compared to the firing rate of the original FS. (Kruskal-Wallis one-way ANOVA, $p < 0.0001$. FS vs nbFS (paired data): post-hoc Wilcoxon signed rank test with Bonferroni correction, $p < 0.001$; nbFS vs GC (non-paired): post-hoc Mann-Whitney U-test with Dunn-Sidak correction, $p = 0.02$; FS vs GC (non-paired): post-hoc Mann-Whitney U-test with Dunn-Sidak correction, $p < 0.001$).

(E) Distributions of R_{output} (τ_w = 10ms). Data points correspond to individual recording sets of nbFS (purple) or GC (green). Both distributions are still significantly different, suggesting the bursting behavior of FS is not sufficient to explain the difference in pattern separation (Unbalanced two-way ANOVA. Stimulation groups: $p = 0.002$, cell-types: $p < 0.0001$, interaction: $p = 0.84$. Post-hoc Tukey-Kramer tests: nbFS and GC R_{output} are significantly

different ($p < 0.05$) for stimulation groups with measured correlation R_{input} = 0.88, 0.84, 0.74.)

(F) Distributions of R_w (τ_w = 10 ms) are still significantly different between GC and nbFS (unpaired T-test, $p < 0.0001$). This suggests the bursting behavior of FS is not sufficient to explain the difference in spiketrain reliability R_w.

(D-F) Asterisks signify $p < 0.001$.

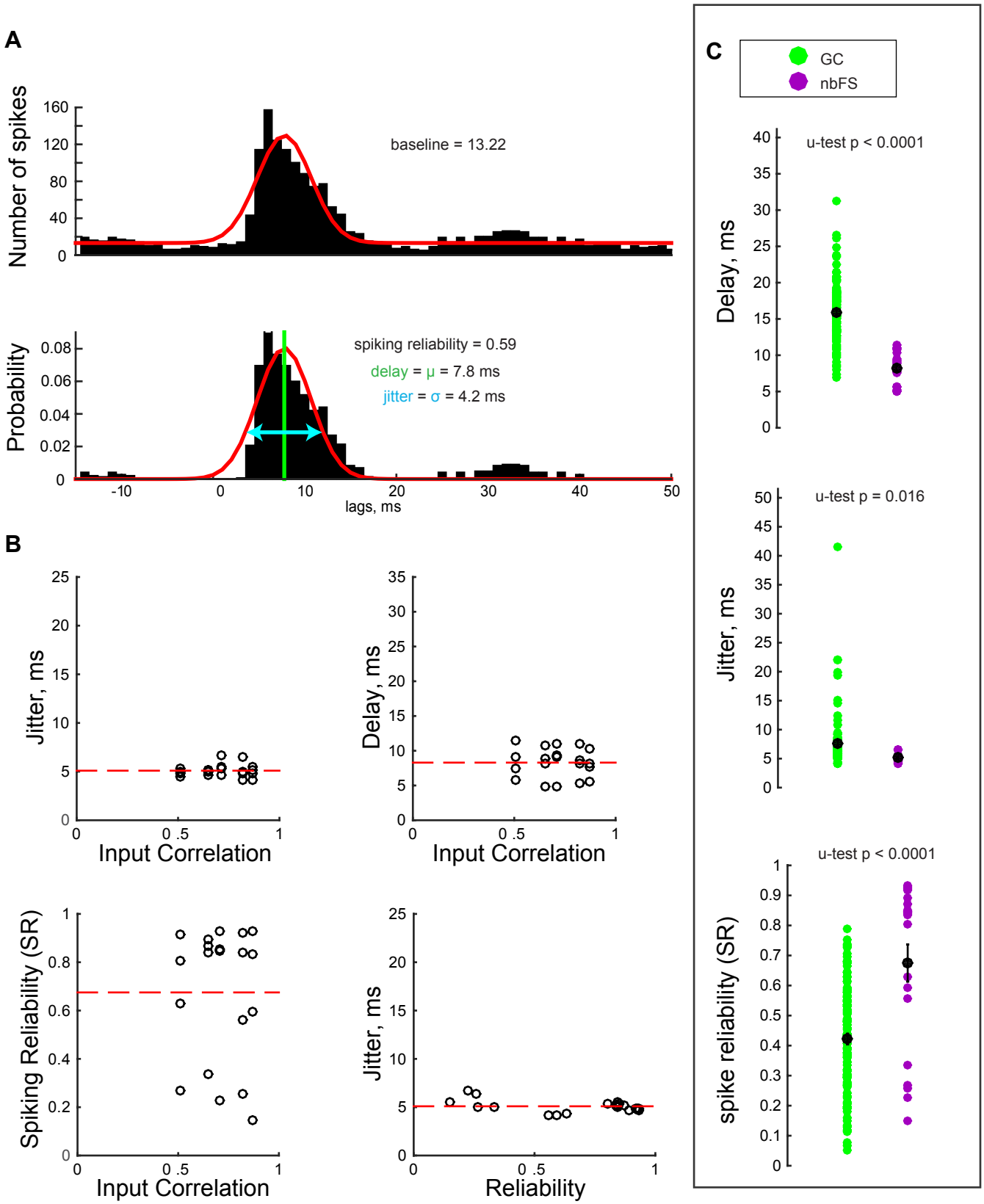
A
Number of spikes
baseline = 13.22
Probability
spiking reliability = 0.59
delay = μ = 7.8 ms
jitter = σ = 4.2 ms
lags, ms
B
Jitter, ms
Input Correlation
Delay, ms
Input Correlation
Spiking Reliability (SR)
Input Correlation
Jitter, ms
Reliability
C
GC
nbFS
Delay, ms
u-test p < 0.0001
Jitter, ms
u-test p = 0.016
spike reliability (SR)
u-test p < 0.0001

Figure S8

Figure S8 related to Figure 7. Fast-spiking interneurons and granule cells have different noise characteristics.

(A) Cross-occurrence method (same as in **Figure S3**) to measure spike delay, jitter and spiking reliability of nbFS neurons (to only consider the noise characteristics of the first spike, if there is a burst) *Top*: example of a histogram representing the number of output spikes occurring after input spikes. The histogram is fitted (red curve) with a Gaussian distribution N(μ,σ, baseline), where μ is the mean delay and σ is the jitter of this delay. Lag 0 ms corresponds to the input spike time. In this example, output spikes are generated on average 7.8 ms after an input spike (delay) with a jitter of 4.2 ms. *Bottom***:** the baseline is subtracted and the histogram divided by the number of input spikes during the recording session. This gives the distribution of the probability of spiking after an input spike of the cell during the recording session (SR). Here the neuron fires 59% of the time after an input spike.

(B) Delay, jitter, and SR distributions for the 20 nbFS recording sets. Dashed horizontal black lines represent means. To compare with **Figure S3**.

(C) Comparison of the delay, jitter and SR between nbFS and GC recordings (Mann-Whitney U-tests, $p < 0.0001$). FS first spike responses to a stimulation impulse is faster, has less jitter, and is more reliable than in GCs.

Statistics table

Figure	Test	N		Descriptive stats	p-value	Degrees of freedom & F/t/z/R/etc value	other
2D	One-sample T-test	8 8 13 13 10 13 11 11 8 4 3	recorded neurons	mean +/- SEM.	< 0.0001 < 0.0001 < 0.0001 < 0.0001 < 0.0001 < 0.0001 < 0.0001 < 0.0001 < 0.0001 0.0002 0.0093	t(7) = 21.81 t(7) = 12.81 t(12) = 22.70 t(12) = 24.49 t(9) = 19.91 t(12) = 33.62 t(10) = 41.62 t(10) = 24.15 t(7) = 20.56 t(3) = 22.28 t(2) = 10.325	Rinput = 1 0.95 0.88 0.84 0.76 0.74 0.65 0.56 0.47 0.26 0.11
2D	Unbalanced one-way ANOVA	8, 8, 13, 13, 10, 13, 11, 11, 8, 4, 3	11 groups of 102 recording sets from 28 neurons	mean +/- SEM	< 0.0001	F(10,91) = 30.05	
2D	Post-hoc Tukey-Kramer Multiple-comparison	8, 8, 13, 13, 10, 13, 11, 11, 8, 4, 3	recorded neurons	mean +/- SEM	see Fig2d right		
2D	unbalanced one-way ANOVA	8, 8, 13, 13, 10, 13,	11 groups of 102 recording	mean +/- SEM	0.19	F(10,91) = 1.42	

		11, 11, 8, 4, 3	sets (see above)				
S1D	one-sample T-test	8 8 13 13 10 13 11 11 8 4 3	recorded neurons	mean +/- SEM.	0.0013 0.0125 < 0.0001 < 0.0001 0.0006 < 0.0001 < 0.0001 < 0.0001 0.0002 0.0107 0.0905	t(7) = 5.17 t(7) = 3.335 t(12)= 6.85 t(12) = 7.65 t(9) = 5.12 t(12) = 9.05 t(10) = 8.08 t(10) = 8.32 t(7) = 7.05 t(3) = 5.69 t(2) = 3.095	Rinput = 1 0.95 0.88 0.84 0.76 0.74 0.65 0.56 0.47 0.26 0.11
3E	one-sample T-test	8 8 13 13 10 13 11 11 8 4 3	recorded neurons	mean +/- SEM.	< 0.0001 < 0.0001 < 0.0001 < 0.0001 < 0.0001 < 0.0001 < 0.0001 < 0.0001 < 0.0001 0.0008 0.0224	t(7) = 19.75 t(7) = 12.07 t(12)= 18.61 t(12) = 19.89 t(9) = 18.32 t(12) = 23.97 t(10) = 35.61 t(10) = 17.85 t(7) = 16.67 t(3) = 14.125 t(2) = 6.58	NDPinput = 1 0.95 0.89 0.86 0.78 0.77 0.70 0.61 0.52 0.32 0.19

3F	one-sample T-test	8 13 13 13 11 10 8 11 4 3 8	recorded neurons	mean +/- SEM.	0.0011 0.0017 0.0013 0.0028 0.0072 0.0020 0.0024 0.0111 0.1408 0.7098 0.1006	t(7) = 5.31 t(12) = 4.015 t(12) = 4.19 t(12) = 3.735 t(10) = 3.36 t(9) = 4.29 t(7) = 4.62 t(10) = 3.11 t(3) = 1.99 t(2) = 0.43 t(7) = 1.89	SFinput = 1 0.9789 0.9722 0.9721 0.9721 0.9542 0.9388 0.9278 0.9062 0.8891 0.8819
4D	one-sample T-test	8 8 13 13 10 13 8 11 11 4 3	recorded neurons	Parabolic best fit	< 0.0001 < 0.0001 < 0.0001 < 0.0001 < 0.0001 < 0.0001 0.00016 < 0.0001 0.0014 0.0546 0.9143	t(7) = 11.37 t(7) = 10.55 t(12)= 9.82 t(12) = 10.255 t(9) = 8.055 t(12) = 10.41 t(7) = 7.25 t(10) = 7.445 t(10) = 4.36 t(3) = 3.07 t(2) = 0.12	SPIKEinput = 1 0.98 0.955 0.92742 0.92741 0.905 0.83 0.827 0.823 0.78 0.74

S2E	linear regression F-test	124950	pairs of spiketrains from 102 recording sets	R^2: 98.0% 4.5% 6.8%	<0.0001 <0.0001 <0.0001	F(1, 124948): 4.8015e+06 4.7031e+03 7.2876e+03	
S2F	linear regression F-test	102	recording sets	R^2: 95.4% 12.3% 20.9%	<0.0001 <0.0001 <0.0001	F(1, 100): 2.0925e+03 14.10 26.36	
5B	One-sample T-test	8 8 13 13 10 13 11 11 8 4 3	recorded neurons	parabolic best fit	< 0.0001 0.0001 < 0.0001 < 0.0001 < 0.0001 < 0.0001 < 0.0001 < 0.0001 0.0001 0.0042 0.1125	t(7) = 11.23 t(7) = 7.43 t(12) = 12.63 t(12) = 16.615 t(9) = 8.57 t(12) = 17.59 t(10) = 13.65 t(10) = 17.72 t(7) = 8.15 t(3) = 7.91 t(2) = 2.72	Rinput = 1 0.95 0.88 0.84 0.76 0.74 0.65 0.56 0.47 0.26 0.11
5C left	two-way ANOVA	102, 102	recording sets	mean +/- SEM	0.145	F(1,192) = 2.14	
5C left	F-test using parabolic regressions	102, 102	Recording sets	mean +/- SEM	0.47	F(3,198) = 0.84	
5C right	one-sample T-test	8	recording sets	mean +/- SEM	0.63	t(7) = -0.51	Rinput = 1

		8 13 13 10 13 11 11 8 4 3			0.09 0.03 0.06 0.96 0.06 0.73 0.46 0.77 0.85 0.60	t(7) = -1.99 t(12) = -2.47 t(12) = -2.06 t(9) = -0.05 t(12) = -2.07 t(10) = 0.36 t(10) = -0.77 t(7) = -0.30 t(3) = -0.21 t(2) = -0.6	0.95 0.88 0.84 0.76 0.74 0.65 0.56 0.47 0.26 0.11
6C	F-test using parabolic regressions	102, 102	Recording sets	parabolic best fits	< 0.0001	F(3, 198) = 18.47	
6D	unpaired T-test	102, 102	recordings sets	means and distribution histograms	< 0.0001	t(202) = 7.94	
6E top	one-sample T-test	102	recording sets	means and distribution histograms in 6d	< 0.0001	t(101) = 22.22	
6E bottom	one-sample T-tests	8 8 13 13 10 13 11 11 8 4	recording neurons	mean +/- SEM	< 0.0001 0.0003 < 0.0001 < 0.0001 0.0002 0.0001 0.0019 0.0007 0.0015 0.1246	t(7) = 15.16 t(7) = 6.49 t(12) = 7.09 t(12) = 7.57 t(9) = 6.06 t(12) = 5.71 t(10) = 4.18 t(10) = 4.86 t(7) = 5.03 t(3) = 2.12	Rinput = 1 0.95 0.88 0.84 0.76 0.74 0.65 0.56 0.47 0.26

		3			0.9688	t(2) = -0.04	0.11
S4B	F-test using parabolic regressions	102, 110	recording sets	parabolic best fit	< 0.0001	F(3,206) = 68.23	
S4C	unpaired T-test not assuming equal variance	102, 110	recording sets	means and distribution histograms	< 0.0001	t(104) = 15.18	
S5A	Linear regression F-test	102	recording sets	R^2: 5.0% 0.6% 9.8%	0.02 0.43 0.0014	F(1,100) = 5.28 0.62 10.83	Jitter Delay SR
S5B	Linear regression F-test	102	recording sets	R^2: 13.3% 7.0% 16.5%	0.0002 0.0073 < 0.0001	F(1,100) = 15.37 7.50 19.77	Jitter Delay SR
S5C	Linear regression F-test	110	recording sets	R^2: 0.2% 0.5% 13.1%	0.66 0.44 0.0001	F(1,108) = 0.19 0.60 16.34	Jitter Delay SR
S5D	Linear regression F-test	102	recording sets	R^2: 11.4% 11.5% 38%	0.0005 0.28 < 0.0001	F(1,100) = 12.82 1.16 61.50	Jitter Delay SR
S5E	Linear regression	20	recording sets	R^2: 15.6%	0.08	F(1,18) = 3.33	Jitter

	F-test			11.8% 56.3%	0.14 0.0001	2.42 23.18	Delay SR
S6A	Linear regression F-test	102	recording sets	R^2 = 6.5%	0.0095	F(1,100) = 7.00	
S6B	Linear regression F-test	102	recording sets	R^2 = 20.5 %	< 0.0001	F(1,100) = 25.75	
S6C	Linear regression F-test	102	recording sets	R^2 = 24.8 %	< 0.0001	F(1,100) = 32.97	
7D	F-test using linear regressions	20, 61	recording sets (FS, GC)	Linear best fit	< 0.0001	F(2,77) = 38.70	
7D	Unbalanced two-way ANOVA	20, 61	recording sets (FS, GC)	Linear best fit	0.016 < 0.0001 0.72	F(4,71) = 4.86 F(1,71) = 69.65 F(4,71) = 0.52	Input groups Cell types Interaction
7D	Post-hoc Tukey-Kramer Multiple-comparison	4, 13 4, 13 4, 13 4, 11 4, 11	Recorded neurons (FS, GC)	R_{output} Mean +/- SEM 0.26±0.05 | 0.12±0.02 0.34±0.04 | 0.17±0.02 0.40±0.04 | 0.18±0.02 0.42±0.04 | 0.21±0.02 0.45±0.04 | 0.23±0.02	0.1977 0.0643 0.0024 0.0032 0.0014		R_{input} = 0.56 0.65 0.74 0.84 0.88

7D	one-sample T-test on difference between R_{output} of simultaneously recorded GC and FS	3 3 3 3 3	Pairs of recorded neurons	Mean +/- SEM -0.4038 ± 0.02 -0.3443± 0.03 -0.3266± 0.03 -0.1683± 0.002 -0.2397± 0.007	0.0024 0.0079 0.0061 0.0002 0.0008	t(2) = -20.23 t(2) = -11.18 t(2) = -12.74 t(2) = -78.87 t(2) = -35.94	R_{input} = 0.56 0.65 0.74 0.84 0.88
7E	unpaired T-test	20, 61	recording sets (FS, GC)	Mean +/- SEM	< 0.0001	t(79) = -8.81	
7E	one-sample T-test on difference between Rw of simultaneously recorded GC and FS	15	Pairs of recording sets	Mean +/- SEM	< 0.0001	t(14) = -28.11	
S7B	Linear regression F-test	61 + 20 = 81	Recording sets (GC + FS)	R^2 = 50.4%	< 0.0001	F(1, 79) = 80.36	
S7D	Kruskal-Wallis ANOVA	20, 20, 61	Recordings sets (FS, nbFS, GC)	Mean +/- SEM	< 0.0001	$\chi^2(2,98) = 23.03$	
S7D	Post-hoc Mann-Whitney U-	20, 61 20, 61	Recording sets (FS vs GC and	Mean +/- SEM	< 0.0001 0.020		

	tests with Dunn-Sidak correction for 3 comparisons		nbFS vs GC)				
S7D	Post-hoc 2-sided Wilcoxon signed-rank test (for paired data) with Bonferroni correction for 3 comparisons	20, 20	Recording sets (FS vs nbFS)	Mean +/- SEM	< 0.0001	W = 210 (signed rank) z = 3.92 (before Bonferroni correction)	
S7E	F-test using linear regressions	20, 61	recording sets (nbFS, GC)	Linear best fits	< 0.0001	F(2, 77) = 30.12	
S7E	Unbalanced two-way ANOVA	20, 61	recording sets (nbFS, GC)	Linear best fit	0.019 < 0.0001 0.84	F(4,71) = 4.72 F(1,71) = 55.04 F(4,71) = 0.35	Input groups Cell types Interaction
S7E	Post-hoc Tukey-Kramer Multiple-comparison	4, 13 4, 13 4, 13 4, 11 4, 11	Recorded neurons (nbFS, GC)	R_{output} Mean +/- SEM 0.24±0.04 | 0.12±0.02	0.3730 0.0710 0.0107 0.0317 0.0075		R_{input} = 0.56 0.65 0.74 0.84 0.88

				0.32±0.04 | 0.17±0.02 0.36±0.04 | 0.18±0.02 0.38±0.04 | 0.21±0.02 0.41±0.04 | 0.23±0.02			
S7F	unpaired T-test	20, 61	recording sets (nbFS, GC)	Mean +/- SEM	< 0.0001	t(79) = -7.50	
S8C	Mann-Whitney U-tests	20, 61	recording sets (nbFS, GC)	Mean +/- SEM	< 0.0001 < 0.0001 < 0.0001	U = 2171 ; z = 5.1 U = 2236 ; z = 6.0 U = 1488 ; z =-3.7	Jitter Delay SR